1975

Lattice parameter changes in thin films.

Angelo. Yializis
University of Windsor

Recommended Citation

Yializis, Angelo., "Lattice parameter changes in thin films." (1975). *Electronic Theses and Dissertations.* Paper 2581.

LATTICE PARAMETER CHANGES
IN THIN FILMS

by

Angelo Yializis

A Thesis
Submitted to the Faculty of Graduate Studies through the
Department of Physics in Partial Fulfillment of the
Requirements for the Degree of Master of Science
at the University of Windsor

Windsor, Ontario
1975

ABSTRACT

Variation of lattice parameters of thin films (generally less than 1000A^{o} thick) has been the subject of many papers over a long time. In many cases the reported results were contradictory and abnormal spacings in very thin films are now generally regarded with reserve. In this work many of the previous experimental difficulties have been eliminated. This thesis is divided in two parts, in which two different sources of lattice constant changes and the conditions under which they occur were investigated. In part one "actual changes" of the lattice parameters are investigated which depend on the mechanical properties of the thin films. Part two examines "apparent changes" of lattice parameters which arise from charges in the surface of insulating thin films. In this experiment the lattice constant of aluminum films was precisely measured as a function of thickness using selected area diffraction and an internal standard.

It has been clearly demonstrated that the aluminum lattice constant decreases with film thickness. The presence of charges on the surface of insulating films was detected by shadow electron microscopy. The effect of these charges on thin films of CaF_2, NaF, LiF and formvar support films was investigated, and apparent changes of the lattice parameters were calculated.

ACKNOWLEDGEMENT

I would like to express my sincere thanks to Dr. N.E. Hedgecock and Dr. M. Schlesinger for their supervision and continual guidance in this project.

I also wish to thank my wife Shirley for both typing this dissertation and providing moral support.

I am indepted to the National Research Council for providing funds for this project and to Dr. A.H. Qureshi for kindly allowing the use of the vacuum evaporator.

TABLE OF CONTENTS

LIST OF FIGURES

LIST OF TABLES

PART ONE

ACTUAL CHANGES OF THE LATTICE PARAMETERS DUE TO MECHANICAL PROPERTIES OF THIN FILMS

CHAPTER 1.

INTRODUCTION

During the last four decades several attempts have been made to detect the differences between the structural properties of thin films (or very small crystals) and those of bulk (or normal size crystals). Such differences are to be expected considering the large surface to volume ratio of thin films. Surface atoms have a different enviroment from those in the interior and therefore changes in the interatomic spacings are expected.

Lennard - Jones and Dent (1) calculated that a surface (100) plane of an alkali halide has an interatomic spacing approximately 5% smaller than a similar plane in the interior of the crystal. Under equilibrium conditions, in order to keep the interatomic distances of the surface atoms the same as those of the interior atoms, the surface must be subjected to a surface tension of +2000 dyn/cm. Nicolson (2) has calculated a surface tension (for an (100) surface of an alkali halide) of the same order, but Shuttleworth (3), using a different method, has obtained a value of -300 dyn/cm for the surface tension in (100) alkali halide planes. According to the sign of the surface tension the lattice will undergo a compression (positive surface tension) or an expansion (negative surface tension).

For small crystallites the pressure P reaches considerable values. For example, when the surface tension T =1000 dyn/cm and the radius of the crystallites r=20A^{o} then $P=10^{10}$dyn/cm^{2} $\simeq 10^{4}$kg/cm^{2}, that is the particle is under a pressure of 10,000 atm from the surface. Under such pressure, assuming that the compressibility coefficients of the film are the same as those of the bulk, the relative compression of the particles is 3-5%, which corresponds to a change in the lattice constant of several hundredths of an angstrom. Such changes can be easily observed by electron diffraction.

The variation of lattice parameters with crystal size and film thickness has been the subject of a steady stream of research papers over a lengthy period and contradictory results have been reported by apparently careful workers. A literature review and a critical examination of these reports is presented in chapter 2.

The present work describes an experimental approach to the determination of the variation of lattice parameters of thin aluminum films with film thickness. Electron diffraction micrographs were taken of Al films evaporated on a thallous chloride film which was used as an internal standard.
The line profiles of the electron diffraction rings were studied and corrected for background intensity due to inelastic scattering, and the formvar support film. It was found that

the lattice constant of Al decreases with film thickness. This was attributed to the effect of a surface stress and an intrinsic stress acting on the individual Al crystallites in the film. A study of the line broadening of 50A° aluminum films showed that the broadening is mainly due to the crystallite size. This led to the calculation of a surface stress of 1500 dyn/cm which is believed to be responsible for the major part of the volume contraction in Al films of this thickness. In general the work embodied in this part of this dissertation deals with "actual changes" in the lattice parameters of the films due to mechanical properties of these films.

CHAPTER 2.

LITERATURE REVIEW

2.1 Existing Evidence For a Change In Lattice Constant.

One of the first experimental studies of small crystals was conducted by Finch and Fordham (1936) (4). They examined vacuum evaporated alkali halide films by electron diffraction. Gold leaves and colloidal graphite were used as standards. They found that the lattice constants were smaller than those of the bulk and claimed that this effect was due to a positive surface tension.

N.A. Shishakov (51) using electron diffraction techniques observed a decrease in lattice constant . He also made the hypothesis that crystallites in thin films undergo a volume compression as the result of the surface tension. However, Boochs (5) determined the lattice constants of four alkali halides by comparison with evaporated gold films and found that the values were in agreement with the x-ray values within ± 0.15%.

Gnan (47) determined the spacing of NaCl using Bi films as standards and found a +0.2% difference. Pickup (6) also worked on NaCl films and found a +0.7% difference in the lattice constant (in comparison to the x-ray values). Finch, Wilman and Cosslett (75,76) observed similar discrepancies in the lattice constant of ZnO, determined by electron diffraction in terms of gold. At this point it should be noted that the thinned gold foils that were used by the various workers, were determined by x-ray diffraction and found to have a lattice constant 0.4% less than that of the bulk.

F.W.C. Boswell (7) is the first worker who has made precise and extensive measurements. Boswell examined the lattice constants of several alkali halides by electron diffraction with an experimental error of 0.05%. As standards, he used graphite and thallous chloride. The size of the crystals was deduced from the breath of the diffraction rings. The lattice constants of crystals of sizes greater than $150A^{o}$ were found to agree with the x-ray values within the experimental error. For crystals of size less than $100A^{o}$, the lattice constants were found to decrease by an amount proportional to the diameter "D" of the crystallites. For $D=20A^{o}$, the decrease was 0.5%. Similar effects were observed for evaporated gold films; for $D=30A^{o}$ the decrease in lattice constant was 2.0% and 0.2% for crystalites with $D=40A^{o}$. Boswell also worked on evaporated films of silver and bismuth, and found that in all cases the lattice constants were less than the x-ray values. Boswell's results for the change of lattice constant in LiF when plotted versus 1/D give a straight line, the slope of which corresponds to a surface tension of +2400 dyn/cm.

On the other hand Halliday, Rymer and Wright (8) using a different electron diffraction technique, obtained a value of

-750 dyn/cm for the surface tension of LiF, indicating an increase of the lattice constant.

Yu.F.Komnik (9) examined evaporated films of Ag, Al, Pd and Bi by electron diffraction and found that in all cases the lattice constant decreased monotonically as the film thickness decreased. Komnik also observed that the lattice constant decreases considerably when the size of the crystalites, approaches some critical thickness. This is the thickness at which the film becomes continous.

A.Cimino has measured the lattice constant of sputtered MgO films prepared in air and vacuum, using x-ray techniques. He found that the lattice parameters decreases with increase in preparation temperature, and with increase in crystallite size. With D=88± 10A° the change was + 0.14% and it decreases towards zero as the crystallite size increased to 150 A°. Vook, Parker and Wright (10) measured the lattice parameters of thin evaporated tin films by x-ray diffractometer techniques as a function of film thickness. It was found that the lattice parameter perpendicular to the surface of the film increased as the film thickness increased. Similar measurements by Vook and Otooni (11) on very thin gold films revealed similar results.

More recently Mays, Vermaak and Kuhlmann - Wilsdorf (12) used electron diffraction to determine the surface stress in gold. They used the most recent experimental techniques and took great care in specimen preparation in order to avoid inconsistencies associated with chemical impurities and poor choice of internal standards. They reported a decrease in the lattice constant proportional to the size of the crystallites. Their interpretation of this effect was a surface tension +1175 ±100 dyn/cm. This result was later supported by D.C. Smart and F.W. Boswell (13) using precision selected area diffraction by which the lattice constants of single crystal gold platelets were determined with an accuracy of ±0.03%. The lattice parameters in the (111) plane were found to be less than the bulk value by amounts ranging from 0.28 to 0.04% for crystal thickness 80 - 400A°. The plot of lattice constant versus the reciprocal of the platelet thickness was a straight line, the slope of which corresponds to a surface stress +1070 ± 75 dyn/cm which is consistant with the observed decrease in the lattice constant.

This concludes a small summary of the existing evidence of the change of the lattice parameters in thin solid films.

2.2 Discussion

From the already existing evidence it becomes obvious that the change in the lattice constant of thin films is a real effect and in most cases it deviates from the bulk x-ray value as the size of the crystallites decreases.

In most cases of continous films, the change of the lattice constant does not exceed 0.5% and the accuracy of the results is considerably high, (the highest one reported using conventional diffraction techniques, is 0.03% (13))

For discontinuous films, changes up to 2.8% have been reported (45) (46). However, the interpretation of the diffraction patterns becomes increasingly difficult with diminishing crystal size. So much so, that some serious doubt has been expressed (14), (15), (16) about the validity of some of these measurements. A critical examination of these reports leads to the following conclusions.

In most cases the contradictory results can be explained in terms of preparation techniques that would be considered unsatisfactory by today's standards, in that the specimens were contaminated while prepared (at low vacuum), and not highly pure.

In general the variation of the lattice parameter with film thickness, (or crystallite dimension), has at best, been demonstrated only in a semi-quantitative way, due to experimental difficulties. In most reports, it is difficult to judge the major sources of error due to the limited information presented. However the following factors appear to be the most important.

(1.) A sharply sloped background: For very sharp peaks the effect of the background has been considered negligible. For the case of relatively broad peaks, the change of slope of the background across the half width of the peak is sufficient to cause an appreciable shift of the position of the maximum in the direction of greater background intensity.

(2.) Difficulty of visually locating the true centre (maximum density) of a diffraction peak: It was observed (48) that the lattice parameters determined by visually measuring the ring radii with a travelling microscope were consistently lower than those obtained from microphotometer records. It was also shown (48) that this discrepancy is due to the

(3.) Overlap of tails of adjacent peaks: Archard (49) showed that when two peaks occur in close proximity, there may be overlapping of their tails, thus introducing shifts of their maxamina.

(4.) Spotting of the diffraction rings: If in a sample there is an insufficient number of crystallites to give a uniform distribution in orientation, the diffraction rings appears spotty and uneven. This may cause large errors in the determination of the maximum as read from microphotometer records.

In addition to these, Rymer (50) mentioned the following sources of error:

(5.) The intensity is higher on the inner side of a broad ring owing to the shorter perimeter into which the scattered electrons are connected. Due to this effect the maximum is displaced inwards.

(6.) Charging of the photographic plate results in an increase of the ring diameters inversely proportional to their original value.

(7.) An electric charge on the specimen changes the scale of the diffraction pattern. This factor is examined in detail in the second part of this work.

When only the results of the workers who had taken special care to eliminate any of the above sources of errors are considered, the evidence is strongly in favour of a lattice contraction in thin films of metals, alkali halides and oxides. Now the question is: How, and according to what formulated theory can these results be best explained?

There seems to be a relative discrepancy between some of the existent theories and the experimental results. This is not surprising considering the large number of variables involved, most of which are extremely hard to determine. In the next chapter an attempt is made to summarize and classify most of the main factors that cause the change of the lattice parameters in thin films.

CHAPTER 3.

EFFECTS AND MECHANISMS RESPONSIBLE FOR THE CHANGE OF THE LATTICE CONSTANT.

3.1 Crystallite Size Effect And Film Thickness.

As was already noted in the previous chapter, the lattice parameters of thin films depend on the diameter D of the crystallites (7), (8), (9), (46), (47).

The relationship that connects the fractional change of the lattice constant with the diameter of the crystallites has as follows.

Expanding the volume V(p) of the crystallites into a series and neglecting second and higher order terms we have,

$$V = V_o + \frac{\partial V}{\partial P} P$$

$$= V_o - K V_o P$$

where Vo: Volume of crystallite in absence of strain,

$$K = -\frac{1}{V_o}\left(\frac{\partial V}{\partial P}\right)_T$$ is the coefficient of isothermal compressibility,

and P is the pressure

We may write p in the form $\gamma \sigma / r$ where σ is the surface tension, r is the radius of the crystallites and $\gamma = 2$ for spherical particles and $\gamma < 2$ for particles of any other shape.

The fractional change in volume is:

$$\frac{V_o - V_P}{V_o} = \gamma \frac{K\sigma}{r} \qquad (3.1)$$

Therefore for crystals of cubic symmetry the fractional change of the lattice constant is:

$$\frac{\Delta a}{a} = \gamma \frac{K\sigma}{r} \qquad (3.2)$$

Equation (3.2) is a classical expression and applies to individial particles that are subjected to a uniform surface tension. It applies to particles of a definite shape, and it does not account for interactions between specimen and substrate (i.e. interfacial strains), grain boundary stresses, or any deviations in the value of the coefficient of isothermal compressibility from bulk values. Therefore relation (3.2) is not appliciable to thin continuous films. For this reason interpretation of results for continuous films that were based on relation (3.2) are very often in disagreement. Cimino (17) observed a 1/D dependence of the lattice constant of sputtered MgO prepared in vacuum, and a reciprocal variation when the sputtered MgO films were prepared in air. The effect was attributed to the presence of absorbed water which forms an external layer of magnesium hydroxide, and subsequently it creates interfacial strains. Similarly Boswell's (7) results on the surface stess of LiF films were of opposite sign to Halliday's results (8). No explanation has been given for this contradiction. But whatever the cause, it would seem improbable that it can be explained in terms of the factors involved in relation (3.2). This indicates that the surface tension alone, acting on crystallites of polycrystalline thin films, cannot account for all observed changes of the lattice parameters.

A dependence of the lattice constant on crystallite size would be expected to appear also as a thickness dependence. In order to establish a relation between the thickness of a thin film and the change of the lattice parameter, Vook (10) conducted x-ray diffractometer studies on partially oriented Sn films. Vook observed an increase in lattice constant propotional to $1/\sqrt{t}$, where t is the thickness of the film.

Similar studies (11) on gold films indicated an increase in lattice constant proportional to "t". Therefore, no empirical relationship that involves the film thickness can be formulated, unless the film is strain free, and the film is deposited as stack of separate monolayers rather than by a three dimensional nucleation process.

3.2 Effects Due To Stresses

It is well known that the presence of stress in thin films produces considerable effects on their mechanical, electron - transport, magnetic, superconducting and optical properties. This section examines the mechanical effects related to the change of the lattice parameters and it will be divided into two categories, induced strains and residual strains.

3.2.1 Induced Strains

Induced strains are strains induced in the films by external forces. These are mainly thermal strains that the films experience from the difference between the thermal expansion coefficients of the film and the substrate when their temperature is changed.

These strains have been calculated theoretically (18), (19) for thin polycrystalline films. The calculations were checked by x-ray diffractometry for copper and gold on glass substrates (18), and good agreement was observed. It must be noted that in these calculations the variation of the elastic constants was not taken into account. Hoffman (20) indicated that although the temperature pulses in the neighbourhood of the arriving particles are of the order of several hundred degrees, the relaxation times are extremely short (10^{-9} - 10^{-12} sec) and therefore generation of strains by conventional differential thermal expansion is highly impropable. This was supported by Blackburn and Campbell (21) as well as Pashley (22) who experimentally showed that the heat pulses are quickly dissipated and the condensed particles are approximately at the substrate temperature. According to this the differential thermal strains are expected to be very small.

Experimental results (20), (23) show that for unannealed films the thermal strains are only a few percent of the total strain.

Another type of induced strain is that produced by collision of the evaporated particles with a cooled substrate. The particles are frozen into position by loosing their thermal energy. Shear forces can be developed at the film - substrate interface. There are several experimental results that indicate that the change in lattice constant is due to thermal stresses (11), (22), (23). Vook and Otooni (11) reported that annealing and subsequent cooling creates a stress of -0.1% to -0.2% (and a change in lattice constant of - 0.1% to -0.2%) for a corresponding film thickness of 100 - 850A°.

3.2.2 Residual Strains:

Residual strains are the strains which cannot go to zero by removal of the external forces. There are several sources of residual strains and they will be discussed separatly.

(i) Surface Pseudomorphism - Lattice Misfit - Interfacial Dislocations.

Surface Pseudomrphism is the costraining of the deposit to fit the substrate lattice. F.L. Frank and Van der Merwe (24) and later Van der Merwe (25 - 28) developed a theory according to which epitaxial films in the minimum energy configuration are homogenously strained. That is the total energy of the film is reduced by the formation of interfacial dislocations which reduces misfit between the deposit and the substrate at the expense of introducing an elastic strain into the film. If the misfit is small, the deposit lattice is strained to fit the substrate up to a thickness of few hundred angstrong, when the misfit is higher than a critical value, interfacial dislocations are introduced. The critical value of misfit is estimated to vary up to 13% for a "soft" film which is tightly bonded to the substrate down to 0.04% for a "hard" film with weak bonds to the substrate.

Jones (29) made a detailed examination by field emission microscopy of the behaviour of the first few monolayers of copper evaporated onto tungsten. He observed that the first three atomic monolayers were pseudomorphic and reported that this results were consistant with Van der Merwe"s theory. Further verification of Van der Merwe's theory was given by Matthews (30) and Jesser and Matthews (31-34).

(ii) Surface Layers:

It has been observed (35 - 38) that oxide layers on film surfaces produce compressive stresses that increase as the thickness of the oxide layer increases. Halliday (35) reported a compressive oxide on the surface of copper films. He evaluated the stress for oxide layers of different thickness by thinning the oxide chemically and observed a decrease in stress as the layer thickness was reduced.

Another type of surface layer suggested by Gimpl (39) is an amorphous layer that can exist at both the intersurface and the free surface. These layers can be surface oxide layers or intersurface pseudomorphs of the deposit.

(iii) Surface Tension:

Under the assumption that the film is free of any other types of stresses many researchers have related the change of lattice constant with the surface tensions of the free surface and the film - substrate interface.

Halliday and Rymer (8), attributing the line profile of the (220) reflection entirely to the size of the crystallites, found the surface tension of lithium fluoride $T = 750$ dyn/cm, where $T = -\frac{1}{2}p(0.91)(\lambda L)/W$, $p =$ Hydrostatic presure, $W =$ linear width of the diffraction rings, and they assumed a cylindrical crystallite shape with the main axis of the cylinders perpendicular to the substrate. With no doubt a number of objections can be raised with respect to the validity of the various assumptions.

More recently Mays (12) reported a decrease of lattice constant by 0.2 to 0.4% for spherical Au crystals ranging in diameter from 125 to 35 A^o respectively. This variation was interpreted as a surface tension of 1175 dyn/cm. In agreement with these results Boswell (13) calculated a surface tension of 1070 dyn/cm in measuring the lattice spacing of gold platelets (thickness 86 - $400A^o$)

There are various surface tension models (1 - 3), (41), (42), but the value of the surface stress takes realistic values only when the film is discontinous with small isolated crystals, so one can safely conclude that the surface tension in continous films of thickness of the order of a few hundred Angstroms is only a minor factor in the stress behaviour of the films.

(iv) Grain Boundary Stress:

Finegan and Hoffman (43), according to their observation of iron films, have constructed a quantitative model which takes into account the surface tension and the growth processes at the crystallite boundary. The model assumes a film in which at first the crystallites grow as hemispheres until they touch, and then grow as columns with densely packed boundaries. They assumed an average interatomic force which follows Hooke's law for small displacements. The stress at the boundary is then given by $\sigma_x = Ed/(1-\nu)l$ where d is the average atomic relaxation distance, l is the average crystallite thickness, E is Youngs modulus and ν Poisson's ratio. This model fits their results reasonably well. According to their observations the iron crystallites are anchored on the substrate when their size is approximately 10A°. At this stage a contraction of the crystallites occurs. This is of the order of 1% and it is due to the surface stress.

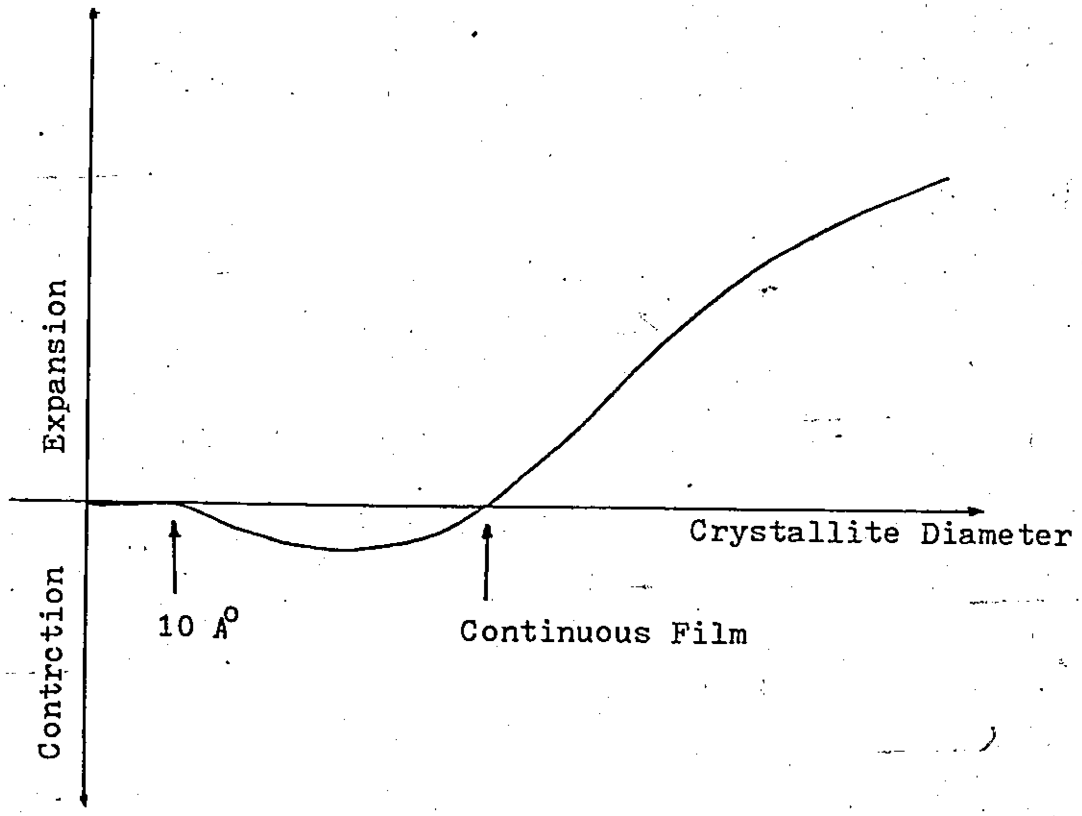

Fig. 3.1 Variation of lattice constant of iron films with crystallite diameter.

This contraction reduces to zero when the film becomes continuous. This shows how the influence of the surface tension decreases as the film becomes continuous Further on as the still existing gaps are closed, a sharply increasing tensional stress is created which results in an expansion of the crystallites (and hence an increase in lattice constant) see figure 3.1 .

This model also permits a qualitative consideration of the effect of condensation rate and substrate temperature on nucleation and crystallite size. But it excludes the possibility of a compressive stress when the film is continous, since it ignores the possible presence of any stacking faults or dislocations that could produce compressive stresses in the film midstructure and superstructure.

(v) Point Defects - Stacking Faults:

Point defects are disturbances which, apart from the plastic strains associated with them, extend for no more then a few interatomic distances. There are two main types of point defects. The first is a vacancy, representing an atomic site from which an atom is missing. The second is called an interstitial defect and consists of an extra atom located at a position between normal lattice sites. Point defect migration to free surface and therefore reduction of intrinsic stress can be obtained by annealing;

the stresses involved are generally small and depend on the density of the vacancies or interstitials in the film.

Stacking faults can be produced by dissociation of a dislocation into two dislocations (with smaller Burgers vector) in order to reduce the elastic strain energy in the film. Faults in general have high energy, however, in some cases if the two dislocations are "partials" (i.e. they have a planar fault as they move apart). The fault has a much lower energy. Rymer (44) using electron diffraction has attempted to determine the stress in gold films by assuming an inhomogenous strain rising from a "Frank partial" (or because of their immobility "Frank sessile"). A Frank sessile occurs when a portion of a sheet of atoms parallel to a (111) plane is removed or inserted into the crystal. Assuming that the crystallites are of considerable extent (500 A^o), the line width is due entirely to the stresses produced by the dislocations and only one dislocation occurs per crystallite. Rymer's results for gold films as well as his later results for silver films (52) are in partial agreement with his theory.

CHAPTER 4

EXPERIMENTAL PROCEDURES

4.1 Experimental Methods

The principle aim of this work is:

(a) to obtain an accurate measure of the lattice parameters in thin polycrystalline films.

(b) to study the line profiles of the electron diffraction rings.

(c) to measure the lattice parameter variation with thickness in thin polycrystalline films at room temperature.

This data may then be used to provide an experimental basis for assessment of models and theories of stress and surface tension in thin films. The experiment involves the determination of the lattice parameters of Al specimens of thickness ranging from 50 to 400 Angstroms. In order to carry out this program the following must be considered.

- choice of an internal standard
- preparation of Al film and of the internal standard
- measurement of diameters of the electron diffraction rings.
- study of the intensity distribution of the electron diffraction rings.

4.2. Experimental Equipment

A Hitachi HU - 12 electron microscope was the primary apparatus used in this experiment. One of the characteristic features of the HU - 12 is the high axial symmetry of the magnetic circuit which permits operation under the most favorable conditions on changing accelerating voltage, magnification and focusing without causing misalignment of the optical system.

The HU - 12 was equipped with a goniometer stage (for translation and tilt), and an anticontamination device (known as "cold finger"). Contamination was mainly caused by condensation of hydrocarbon molecules, which emanate from pumping oil and vacuum grease, and eventually reduce to carbon. By cooling the surroundings of the specimen, contamination is reduced. In extreme cases of no cooling and intense radiation, viewing times up to ten minutes may be used before contamination effects are perceptible (i.e. loss of contrast in the specimen).

Film evaporations were performed in a Balzers oil - diffusion pump evaporator at pressures of 10^{-6} to 10^{-7} torr. The vacuum system included a quartz - crystal thickness monitor which controlled the film thickness within 5 - 10% accuracy.

The photographic plates were measured by means of a Jarrel-Ash non recording microphotometer, connected to a Hewlet - Packard strip chart recorder. A discussion of systematic errors is given in chapter 5.

4.3 Choice of Internal Standard

In order to select a standard substance for electron diffraction, certain conditions should be met by the substance:

(i) The material should be easily prepared in a form suitable for electron diffraction. In this work the thin films were prepared by evaporation, hence the standard substance must be such, that it can be evaporated in a form of a thin film.

(ii) When prepared, the diffraction specimen should remain chemically stable, and without physical change, such as increase in crystal size, over a period of several days.

(iii) The crystal structure and lattice constant must be accurately known and independent of the method of preparation.

(i v) The recorded pattern should consist of several sharp rings which can be measured with high accuracy, in order that a good average value of the parameter involved can be obtained.

(v) The standard substance must be stable under electron bombardment.

Several materials have been used as standards by various workers, either in form of a film or a thinned foil. Most of them have been rejected at times for not satisfing all of the above conditions. Thin films of gold were often used, but as it was shown by Vook (11) their lattice constant is not in agreement with the x-ray value. In addition the diffraction rings show considerable broadening due to the lattice imperfections. Many other metals that could be used as standards (Ag, Al, Pb, Bi) behave in a similar way, and hence are considered unsuitable.

Alkali halides have been suggested as standards since most of them are easily evaporated and give good diffraction patterns. The problem here is crystal growth when left in air (such as NaCl), or tendency to form very small crystallites which results in considerable line broadening (as in LiF and CaFi). Fewer objections are raised for the use of certain oxides as standards (such as MgO and ZnO). Thallium chloride has been suggested as a standard by several authors (7, 45, 53). Meyerhoff (53) has investigated TlCl in detail and determined a lattice constant of $a_o = 3.8400 \pm 0.0004$ A° at 20°C for a 300 A° thick evaporated film. Other work has also established that TlCl is a reliable standard. In this work a vacuum evaporated film of TlCl about 150 A° thick was used. The TlCl film was found to provide a standard specimen satisfying all of the above conditions. A typical diffraction pattern of such a film is shown in figure 5.3 .

4.4 Specimen Preparation

Formvar support films 100 A° were prepared on glass microslides. To ensure that the formvar film was flat, special care was needed in mounting the film on the 500 mesh microscope grid.

The formvar film was scribed into 4-5 mm squares while on the glass base, and then the squares were floated off in water. A special tool was made by which the grid was brought under the floating squares and then lifted against the formvar and removed from the water. The grid and the formvar support films were then placed on a finely - shredded filter paper for removal of the excess water. In this manner reproducibly flat support films were obtained.

Thallium chloride films 150 A° thick were deposited by evaporation, on the formvar covered grids. The rate of evaporation was approxiamately 5 A° per second. The aluminum (Al) films under investigation were evaporated on the TlCl films at a rate of 8 - 10 A° per second.

The evaporation rates were chosen high in order to increase the purity and decrease the granularity of the films. The more the film formation is prolonged the greater will be the number of gas molecules impinging on the substrate during condensation. The impinging gas molecules may combine with the condensed Al atoms to form oxides or to be trapped in the film. On the other hand, faster film formation will not only increase the purity, but the texture of the film will be more compact. That is, at high rates of film evaporation, more nuclei are initially formed, which results in the formation of a continous film at a lower thickness than when the evaporation rate is low. This effect was easily observed with gold films evaporated on formvar, see figures 4.1 and 4.2 . Similar observations have been made by Levinstein (54) who conducted a thorough investigation of the structure of evaporated metal films by electron diffraction and electron microscopy.

Thin aluminium films do not lend themselves to the demonstration of this effect since they are highly continuous, as is shown by the fact that they are electrically conductive (ohmic conduction) when only 45 - 50 A° thick (55), and films greater than 300 A° have the same specific conductivity as bulk aluminum (55) .

4.5 Determination of Lattice Parameters

Diffraction patterns of the specimens were obtained in a normal microscope position by selected area electron diffraction (SAD). From this position, Bragg reflections from the crystal lattice of the specimen are focused by the objective lens at the back focal plane of the intermediate lens. An aperture placed in the image plane of the objective lens ensures that only electrons from a specimen area as small as 1 micron in diameter contribute to diffraction pattern.

Thus the diffraction pattern, which for polycrystalline materials consists of a set of rings, is recorded on a

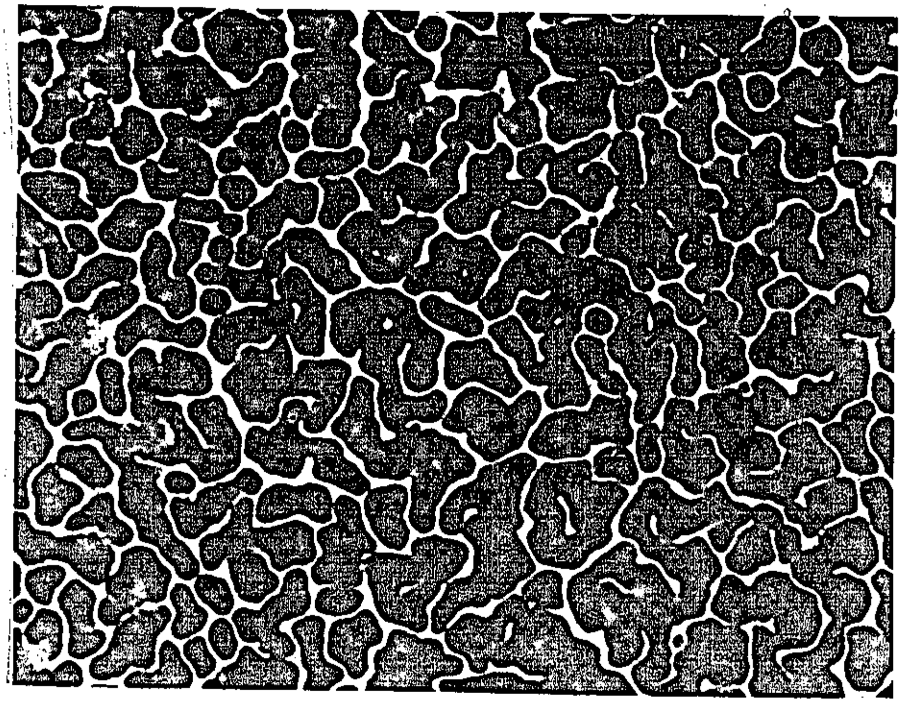

Fig. 4.1 Micrograph a $50A^{o}$ Au film, total evaporation time 100 sec.

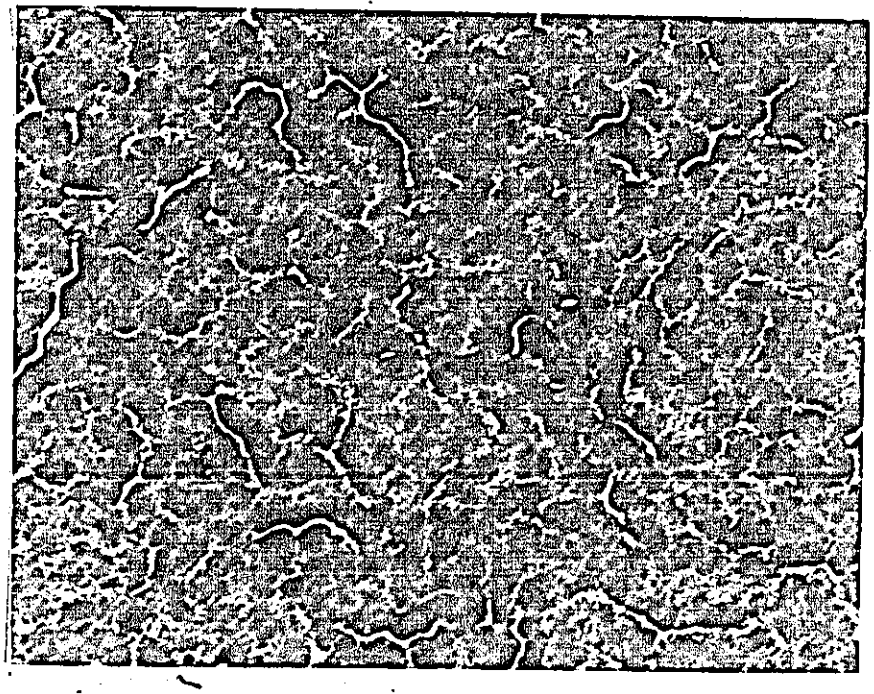

Fig. 4.2 Micrograph of a $50A^{o}$ Au film, total evaporation time 10 sec.

photographic plate. The ring diameters are related to the lattice parameters through the relation.

$$2\lambda L = \frac{D\,a}{\sqrt{h^2+k^2+l^2}} \qquad (4.1)$$

were λ is the wavelength of the electrons

L is the camera length.

a is the lattice constant of the specimen

D is the diameter of the diffraction ring.

h,k,l are the indices of the reflecting plane.

This relation is valid for small diffraction angles for which the approximation $\tan\theta = \theta$ can be used where θ is the angle of diffraction. To a higher order of accuracy, the values of λL will depend on D according to the relation :

$$2\lambda L = \frac{D\,a}{\sqrt{h^2+k^2+l^2}}\left(1 - \frac{3}{32}\,\frac{D^2}{L^2}\right) \qquad (4.2)$$

Calculation of the lattice constant "a" requires the knowledge of the constant λL (known as camera constant). In general practice λL is calculated with the use of a standard film (of known lattice constant) which is inserted in the diffraction chamber before or after the specimen.

This method is not very reliable for high accuracy measurements, since the "effective" camera constant will vary slightly from one determination to another on account of small changes in the position of the specimen, and also due to the hysteresis effects of the magnetic lens.

This indicates that for precision measurements an "internal" standard substance must be used. That is, the standard must be on the same grid with the specimen,

In this manner, the film under investigation was deposited on the standard substance (TlCl), which was deposited as a film on the support film (Formvar), which was originally mounted on the copper grid. Hence a composite diffraction pattern was obtained and the above mentioned errors were eliminated.

4.6 Electron Diffraction Line Profiles

4.6.1 Line Broadening.

(a) Instrumental Broadening.

Many conditions of the experimental methods of recording diffraction lines contribute to their broadening. The electron beam has a finite size, and the collimating system and specimen have a finite width, so there is an angular spread in the electron beam striking the specimen. Other contributions may arise from the finite grain size of the recording film, imperfect focusing and lack of monochromatism of the incident electron beam.

The instrumental broadening can be decreased by various compromises between the factors involved, but it can not be eliminated.

(b) Intrinsic Broadening.

Apart from the above mentioned forms of broadening we may have broadening due to the state of the material in the specimen. This is known as intrinsic broadening and it results from the following sources:

Particle size: If the specimen consists of very small crystals it will not diffract electrons at discrete Bragg angles, hence the diffraction lines will be broadened.

Strains: these can be microstrains or macrostrains. If the specimen is strained it will behave like a mixture of crystallites of varying lattice paremeter and thus the lines will be broadened.

Other forms of departure from perfect periodicity of the crystal structure, (such as stacking fault deformations and various dislocations) can also cause line broadening.

4.6.2.) Interpretation of Intrinsic Broadening.

Fourier analysis of x-ray diffraction line profiles is a proven method for investigating the defect structure of crystalline materials (56 - 58). This method requires fourier analysis of diffraction profiles of multiple orders of a hkl reflection so that effects of particle size and of microstrains can be separated. However, in thin films it is not always possible to obtain multiple order diffraction profiles and the problem of separation of the two effects becomes increasingly difficult.

Several approximate solutions have been given for first order x-ray diffraction profiles (59 - 64) but the problem has not been solved for electron diffraction line profiles. The main difficulty is that most of the information lies in the "wings" of the line, which is difficult to determine with any accuracy in the presence of a diffuse background. However, Rymer has indicated that there is a perceptible difference between the profile shapes due to the particle size and those due to intrinsic strains. He showed that the latter always closely follow a Gaussian form over a wide range of intensity, whereas the former deviate from a Gaussian form at intensities of about 10% of the maximum.

In order to examine the line profiles of the Al films it is necessary to separate the intensity due to the diffraction lines from the background intensity.

The background intensity distribution can be obtained by interpolation using points that lie between "distant" diffraction peaks, to avoid peak tails. But it was found that the formvar support film, in addition to its contribution to incoherent scattering, produced at least 3 perceptible broad rings. In order to calculate the position of these rings, equivalent lattice spacings had to be calculated for each one of them. This was made possible by calculating the camera constant for a formvar diffraction pattern (using a separate standard), and from the relation $2\lambda L=Dd$, the effective spacing d corresponding to each ring was found. Having calculated "d" for the formvar rings we can find their position in the specimen's diffraction pattern.

The formvar rings are the only discontinuities in the uniform background of the specimen's diffraction pattern, which to a first order depends on the incoherent atomic scatter from both the specimen and formvar films. The shape of the line profile can now be studied by plotting a graph of log (I/I_o) versus x^2, where I_o is the intensity at the maximum of the line and I the intensity at distance x from I_o.

CHAPTER 5.

EXPERIMENTAL RESULTS.

5.1 Accuracy of the experimental results.

In an experiment of this type an error analysis is critical to the result produced. The sources of error in this experiment may be categorized into the following groups.

(1.) The accuracy with which the peak of a diffraction line can be determined. There are two sources of error here.

(a.) Random errors resulting from slight variations in speed of the microphotometer.

(b.) Uncertainty in locating the maximum of a diffraction line.

(2.) Errors resulting from absolute calibration of the microphotometer.

The ring diameters were measured with a 1:6 microphotometer scale whose precision was checked by superimposing on the diffraction pattern a glass scale on which the markings were accurate to ± 10 μm. Repeated observations showed that for an average ring (3.5cm) the random error 1 (a) for a single reading was ±35μm. The reading uncertainty 1(b) for an average ring of 250μm half width was estimated to be ±30μm. The errors 1(a) and 1(b) enabled the peak of a line to be located with a standard deviation of $\sqrt{35^2 + 30^2} = 46\mu m$. However, every ring diameter was measured along two directions perpendicular to each other, and every setting of the microphotometer was repeated

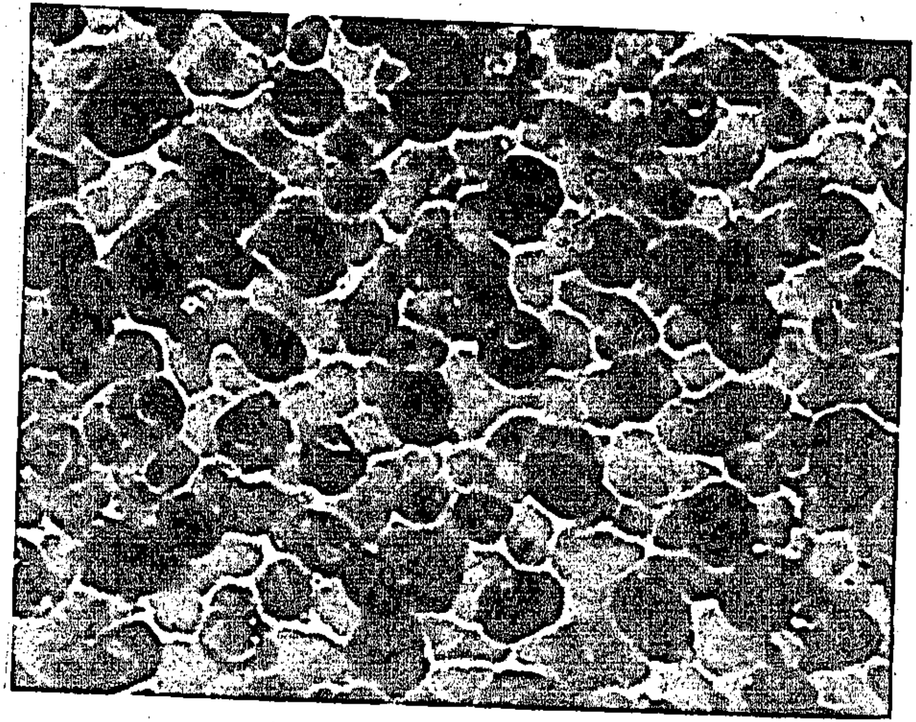

Fig. 5.1 Electron micrograph of a 50 Å aluminum film evaporated on thallium chloride.
Magnification: x 210,000

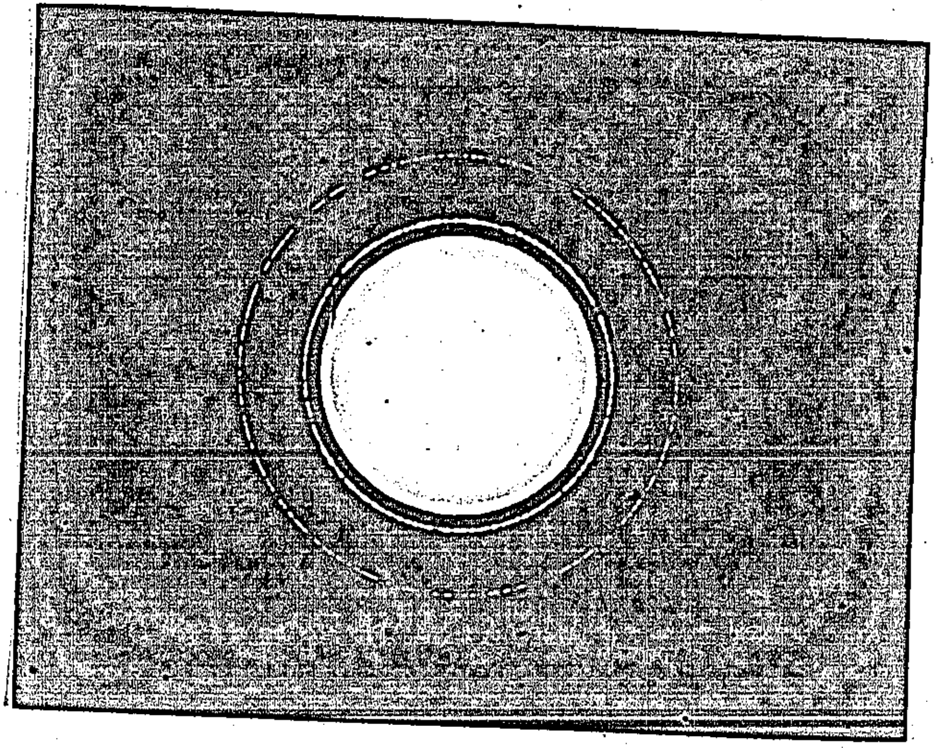

Fig. 5.2 Electron diffraction of a 50 Å aluminum film evaporated on formvar support film.

at least two times, hence the standard deviation of the mean diameter was at most $46/\sqrt{4}=23\mu m$. This represents 3.3 parts in 5000 of the diameter of the average diffraction ring.

The calibration errors (2) result from a combination of the uncertainty in the standard scale and the uncertainty in the movement of the microphotometer, and this is estimated to be $6.3\mu m$ or 0.9 parts in 5000 for an average ring diameter. This is a systematic error common to all observations. Hence the total error for the determination of a ring diameter is $\sqrt{(3.3)^2+(0.9)^2}=3.4$ parts in 5000.

In order to calculate the lattice constant of aluminum for a single Al ring two similar measurements must be made, that is, one for a TlCl ring, in order to calculate the camera constant, and one for the Al ring. Therefore the uncertainty involved is $3.4\sqrt{2}=4.8$ parts in 5000. Hence the determined lattice parameters are in error at most by $\pm 0.1\%$.

5.2 Diffraction and Electron Microscopy.

A micrograph of a 50A° aluminum film evaporated on thallium chloride is shown in Fig 5.1. A typical electron diffraction pattern of an aluminum film deposited on to a formvar support film is shown in Fig 5.2. Fig 5.3 shaows an electron diffraction pattern of a 150A° thallium chloride film vacuum evaporated on formvar.

As mentioned in the previous chapter, the camera constant and the lattice parameters of the specimen are

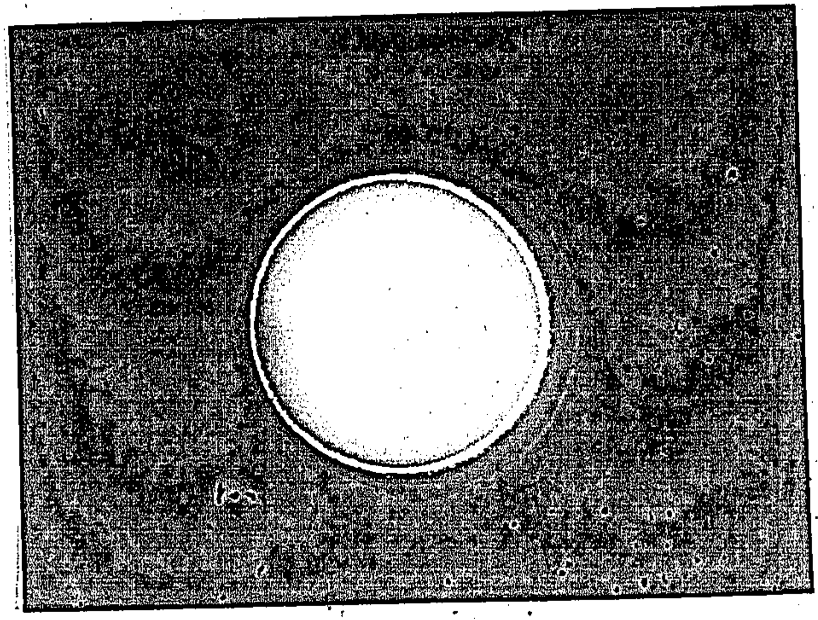

Fig. 5.3 Electron diffraction pattern of a150 Å thallium chloride film, vacuum-evaporated on formvar support film.

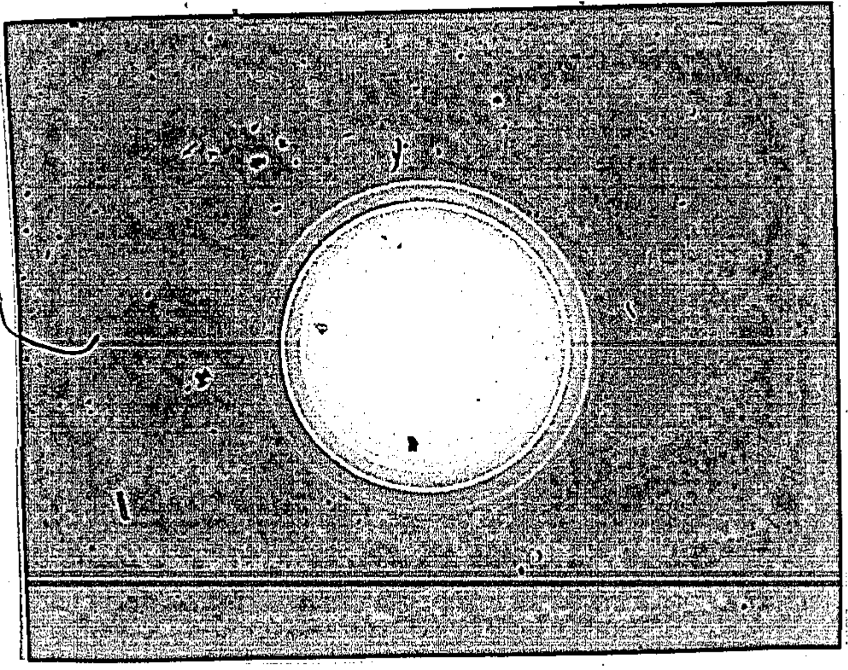

Fig. 5.4 Composite electron diffraction pattern of thallium-chloride and aluminum films.

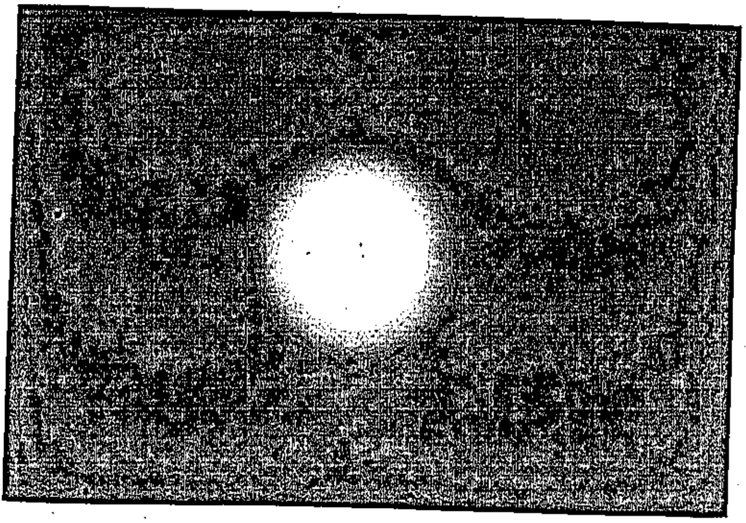

Fig. 5.5 Electron diffraction pattern of a formvar support film.

calculated from a single composite diffraction pattern, that contains diffraction rings from the standard and from the specimen film. Fig 5.4 shows a typical composite diffraction pattern of thallium chloride and aluminum superimposed on a single photographic plate. It should be remembered here that the thallium chloride film is evaporated on to the formvar covered grid, and the aluminum film is subsequently evaporated on to the thallium chloride film. Therefore the diffraction pattern of fig 5.4 should also contain the formvar diffraction rings. These cannot however be seen because they are very broad and of low relative intensity.

The formvar diffraction rings are shown in fig 5.5 . Only two of the three rings can been seen, the third ring is very close to the zero diffraction order, and as it will be seen later it corresponds to large plane spacing "d" and it does not coincide with any specimen reflection.

5.3 Measurement of the Diffraction Patterns.

For the calculation of the lattice parameters - equation 4.2 was used. The camera constant λL was calculated from the TlCl rings, this allowed the calculation of the camera length "L" since the wavelength was known from the accelerating potential of the electrons, which was set at 100KV. The camera constant "a" was then calculated for each of the aluminum rings. Results for aluminum films of various thickness are shown in table 1. A plot of the Al lattice constant versus film thickness is shown in fig 5.6.

The identification of each ring with its corresponding reflection (hkl) was done by plotting $\sqrt{h^2+k^2+l^2}$ versus the diameter of each ring. According to equation 4.1 the points of the graph should lie on a straight line within the limits of the first order correction, which is usually much smaller than the difference in the diameters of any two adjacent rings. Hence points that lie off the straight line are identified wrongly.

The formvar "plane spacings"* are calculated in a less accurate manner due to the broad and of weak intensity diffraction rings. The camera constant was measured by an external TlCl standard and the calculated average values

---

* The term "plane spacings" is used here in the absence of a term that could describe the actual structure of the formvar films for which we have no precise knowledge.

Table 1. Variation of lattice constant of Al with film thickness.

Film Thickness (A^o)	Rings Measured (hkl)	$a_{Al}(A^o)$	Average $a_{Al}(A^o)$
50	111	4.026	4.027
	200	4.028	
	220	4.028	
	311	4.026	
100	220	4.031	4.029
	311	4.027	
200	220	4.031	4.033
	311	4.036	
	331	4.032	
	420	4.032	
350	220	4.049	4.044
	311	4.046	
	331	4.042	
	420	4.040	

Table 2. "Lattice spacings" of a formvar support film.

$d_{formvar}(A^o)$
$d_{1f}=5.53$
$d_{2f}=2.21$
$d_{3f}=1.27$

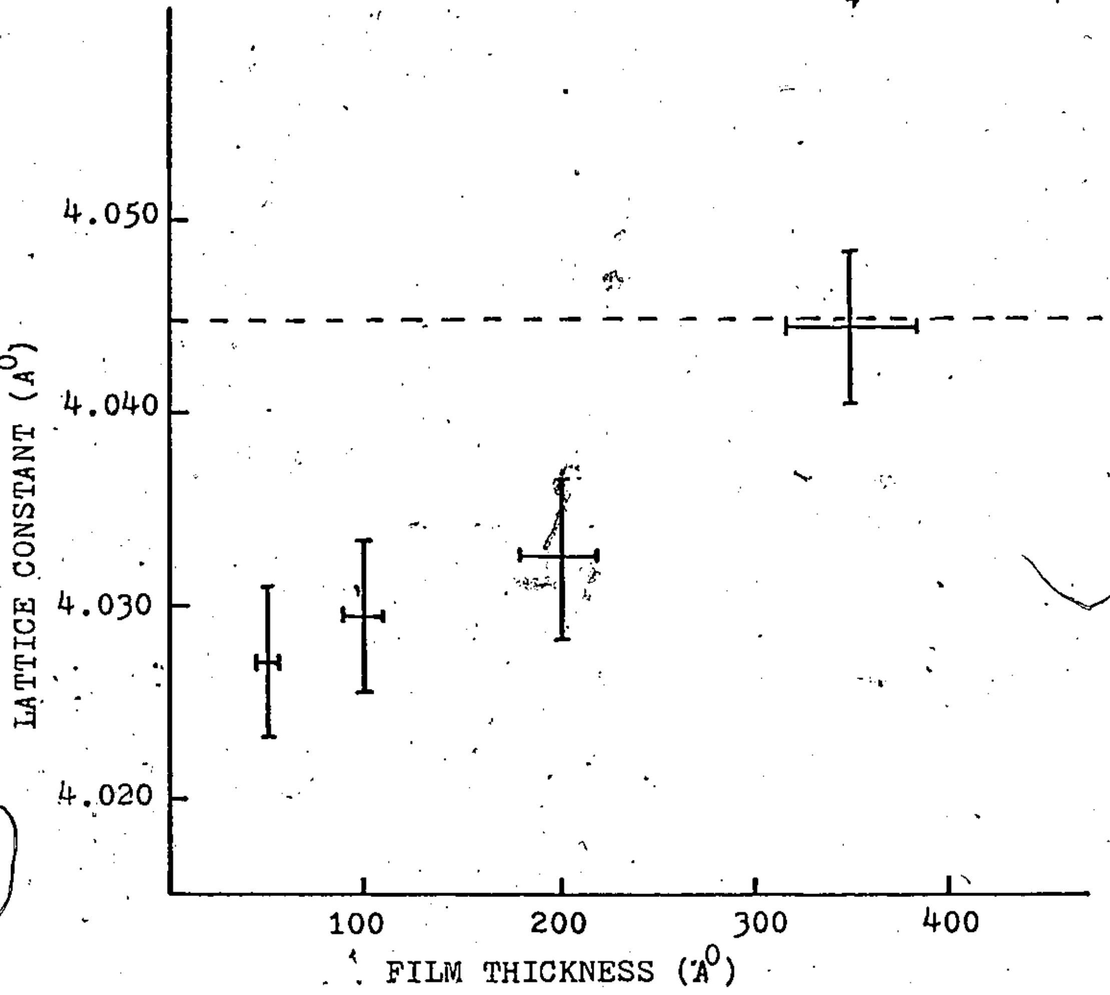

Fig. 5.6 Graph of lattice constant of aluminum films versus film thickness. The dotted line indicates the lattice constant of bulk aluminum determined by x-ray diffraction.

of the "plane spacings" "d" are shown in table 2. As mentioned earlier the value of d_{1f} is high when compared with the largest plane spacing of aluminum (d_{111}=2.34A^o), and its effect as an anomaly in the aluminum background is of no importance. However, the values of d_{2f} and d_{3f} are within the range of the first order lattice spacings of most materials and their effect should be taken into account for any kind of study on line profiles. The individual intensity distributions of the specimen, formvar and undiffracted background, and their combination to produce the final pattern is shown in fig 5.7.

The exposure time for all diffraction patterns was low enough to prevent exposure - saturation of the film. This can be seen in Fig 7, since the saturation of the film far from the centre of the diffraction pattern would require the intensity maximum to lie on a straight horizontal line.

The specimen line profiles can now be studied by dividing or subtracting the total intensity curve by the empirically obtained background.

5.4 Shape Of Electron Diffraction Line Profiles

The diffraction rings studied were those of transmission specimens of aluminum. The highest change in the aluminum lattice constant was observed for the 50A^o films (see table 5.1), hence these films were of greatest interest for line shape analysis.

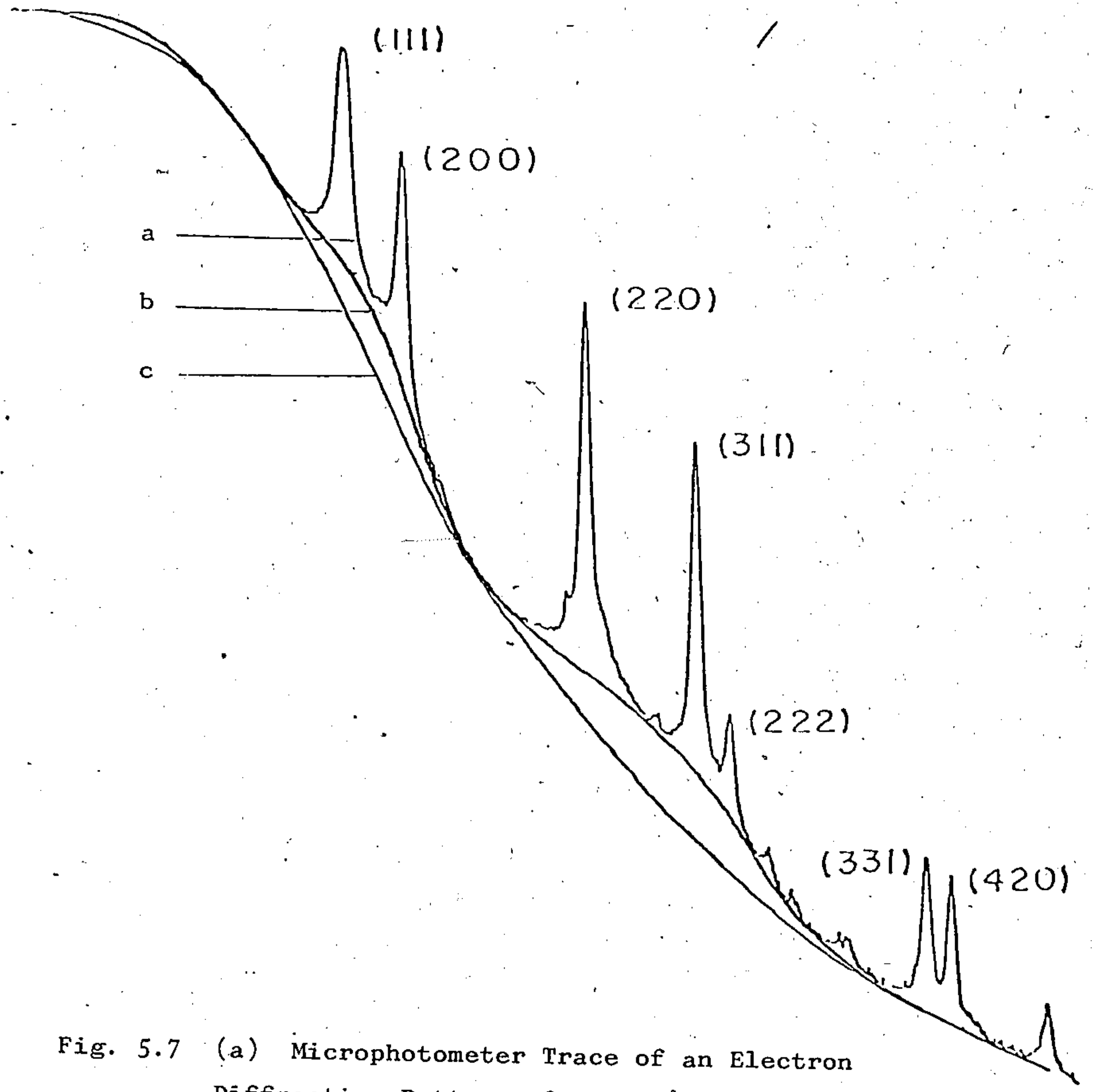

Fig. 5.7 (a) Microphotometer Trace of an Electron Diffraction Pattern of a 200 Å Al Film Deposited on Formvar, (b) Microphotometer Trace of an Electron Diffraction Pattern of a 100 - 150 Å Formvar Film, (c) Intensity Distribution of the Undiffracted Electron Beam.

If instrumental effects are to be negligible, the size of the focused electron beam should not exceed about 10μm(65). A similar limitation applies to the width of the slit of the microphotometer. In this work the beam cross section was 1 - 2μm, and the slit width approximately 1μm.

The backgound intensity was eliminated by direct subtraction, and the contours of the 111, 200 and 220 reflections were tested for Gaussian shape. Figures 5.8 - 5.10 (see also tables 3 - 5) show plots of -log (I/Io) versus x^2 for the above reflections. For a Gaussian line shape, the points should fall on a straight line

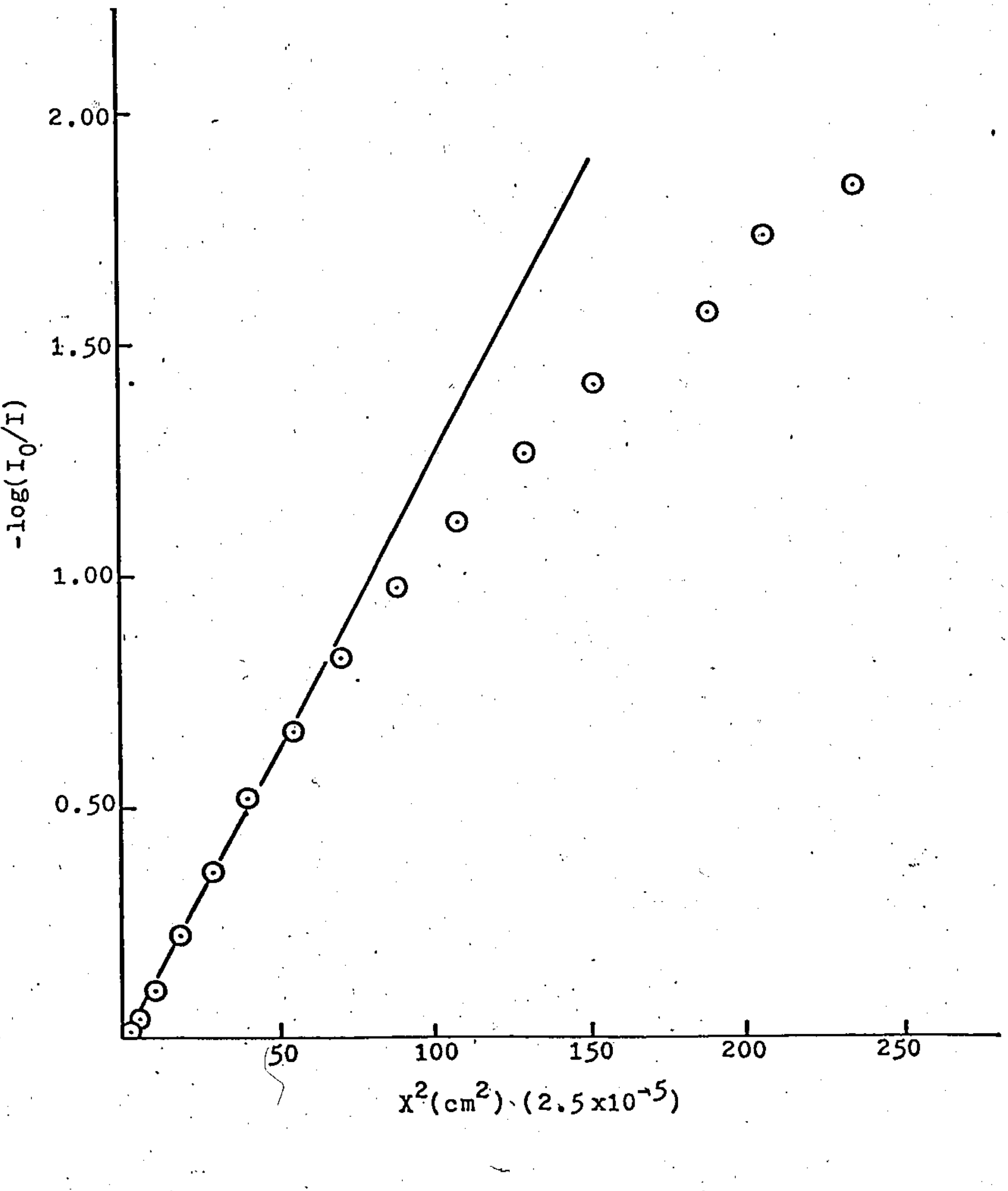

Fig. 5.8 Intensity contour of 111 reflection from a 50 Å vacuum evaporated Aluminum film

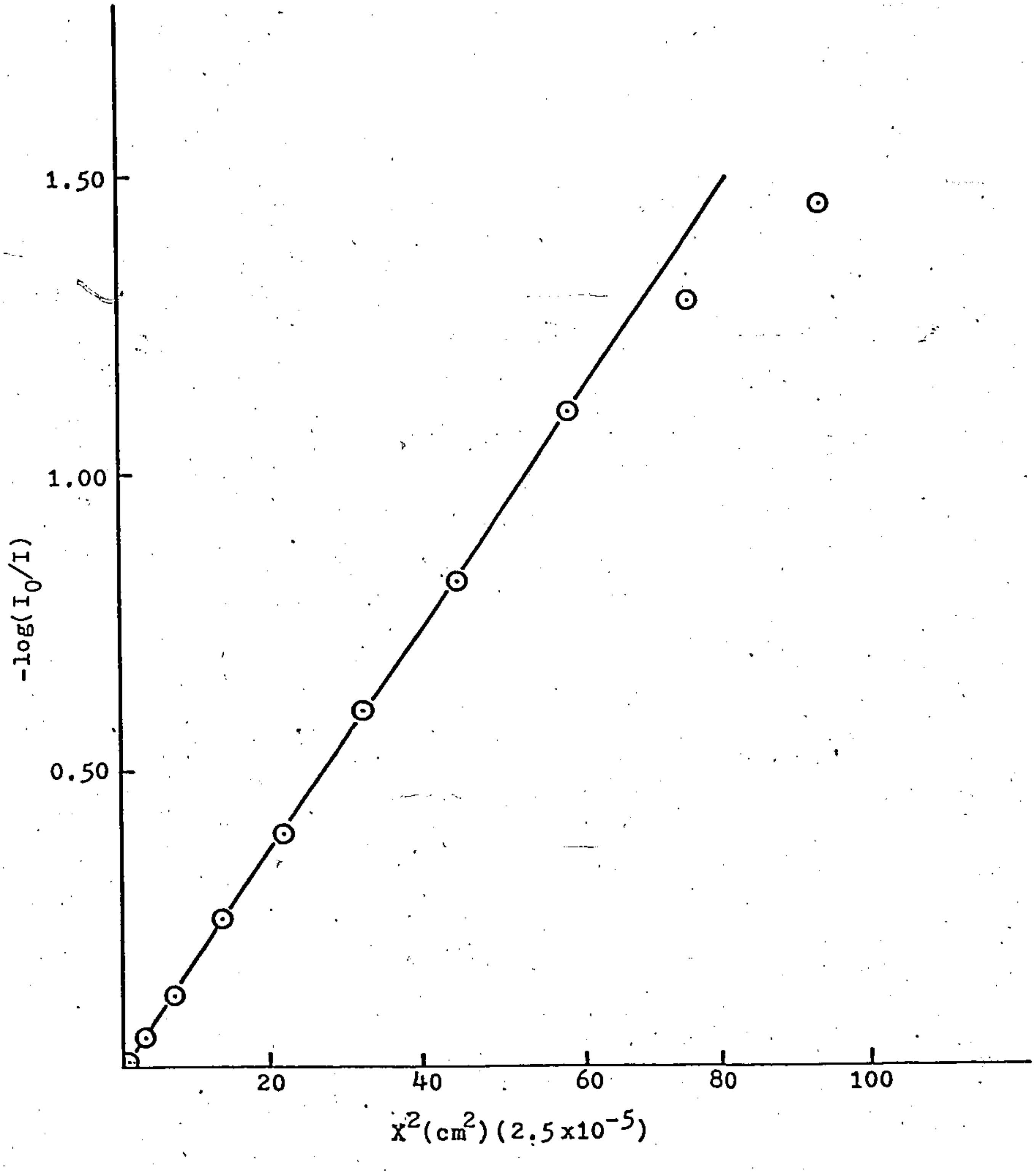

Fig. 5.9 Intensity contour of 200 reflection from a 50 A° vacuum evaporated Aluminum film

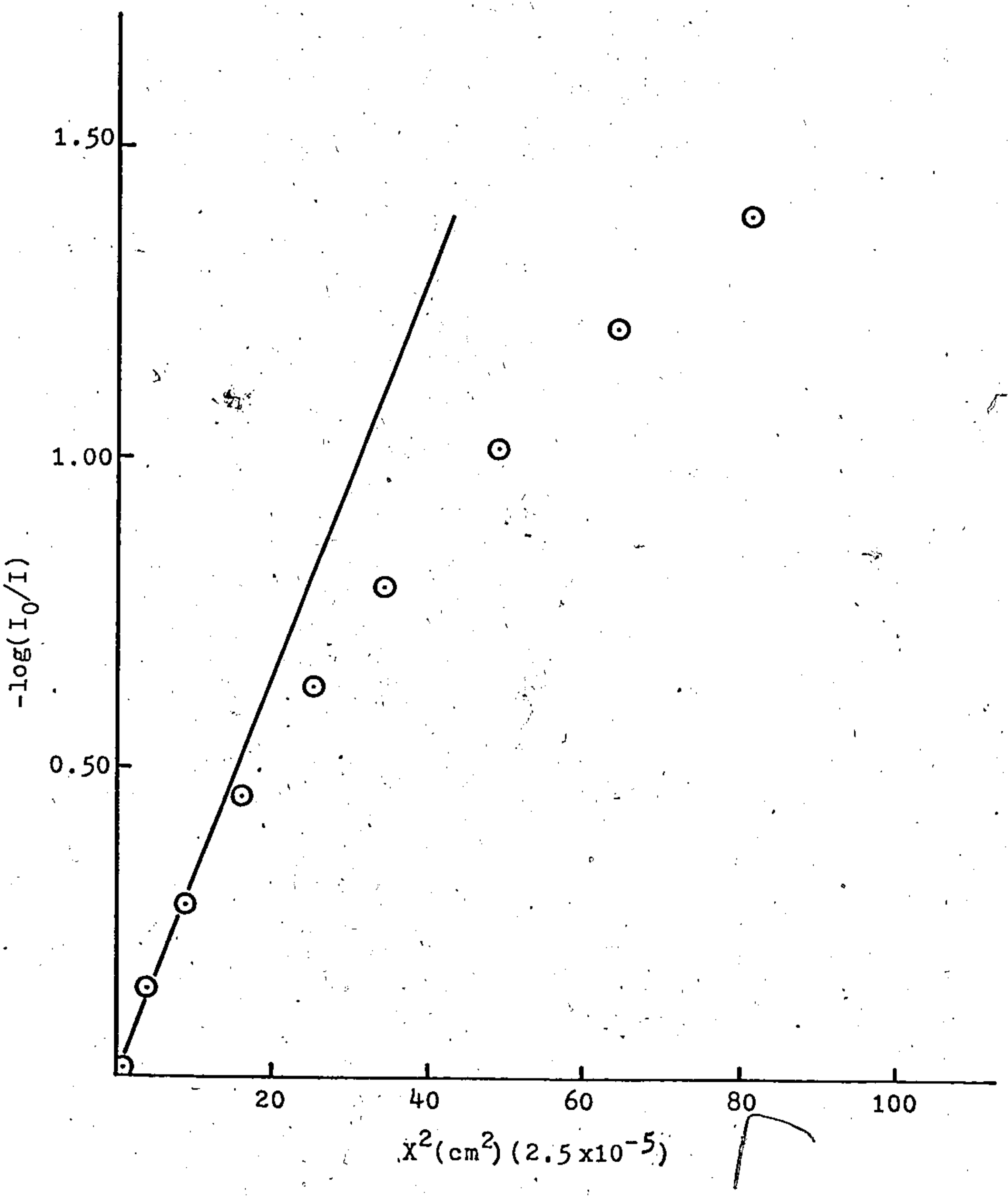

Fig. 5.10 Intensity contour of 220 reflection from a 50 Å vacuum evaporated Aluminum film

Table 3. Analysis of the 200 line profile of a 50 A^{o} aluminum film.

I	X^2(cm^2)x (2.5x10^{-5})	-log(I/I_o)
I_o=5.73	0	0
5.55	0.49	0.01
5.13	2.90	0.05
4.33	7.30	0.12
3.22	13.70	0.25
2.36	22.10	0.39
1.50	32.50	0.60
0.87	44.90	0.82
0.45	59.30	1.10
0.30	75.70	1.28
0.20	94.10	1.46

Table 4. Analysis of the 220 line profile of a 50 A^{o} aluminum film.

I	X^2(cm^2)x (2.5xio^{-5})	-log(I/I_o)
I_o=3.70	0	0
3.50	1.00	0.02
2.68	4.00	0.14
1.96	9.00	0.28
1.32	16.00	0.45
0.87	25.00	0.63
0.63	36.00	0.79
0.35	49.00	1.02
0.23	64.00	1.21
0.15	0.04	1.39

Table 5. Analysis of the 111 line profile of a 50 A° aluminum film.

I	$X^2(cm^2)$x (2.5x10^{-5})	$-\log(I/I_o)$
I_o=12.53	0	0
12.16	1.82	0.01
11.45	5.52	0.04
9.93	11.22	0.10
7.67	18.92	0.22
5.44	28.62	0.36
3.78	40.32	0.52
2.69	54.02	0.67
1.90	69.72	0.82
1.30	87.42	0.98
0.96	107.12	1.12
0.68	128.82	1.27
0.49	152.52	1.41
0.34	178.22	1.57
0.23	205.92	1.74
0.18	235.62	1.84

CHAPTER 6.

INTERPRETATION OF RESULTS AND DISCUSSION

6.1 Variation of Lattice Constant With Film Thickness.

Variations in lattice spacings with crystal size and film thickness has been the subject of a large number of publications over many years. A review of some of the most interesting work has been given in chapters 2 and 3. Results reported in this thesis represent an essentially independent approach which has eliminated most of the important sources of errors that have resulted in the diversity of results as noted previously.

The results on aluminum are interesting in relation to a study of discontinous aluminum films by Yu.F. Komnik (9). Komnik reported a lattice constant decrease ranging from 1% to 4% of the bulk value for spherical aluminum crystallites ranging in diameter from 45A° to about 30A° respectively. It is interesting that the structure of thin Al films (9,55), as well as our results (fig 6.1), show that in film thicknesses up to the value for which the film becomes continous, the crystallites appear essentially circular in electron micrographs. Komnik's results and ours are shown in fig 6.1. It can be observed that the two sets of results combine well.

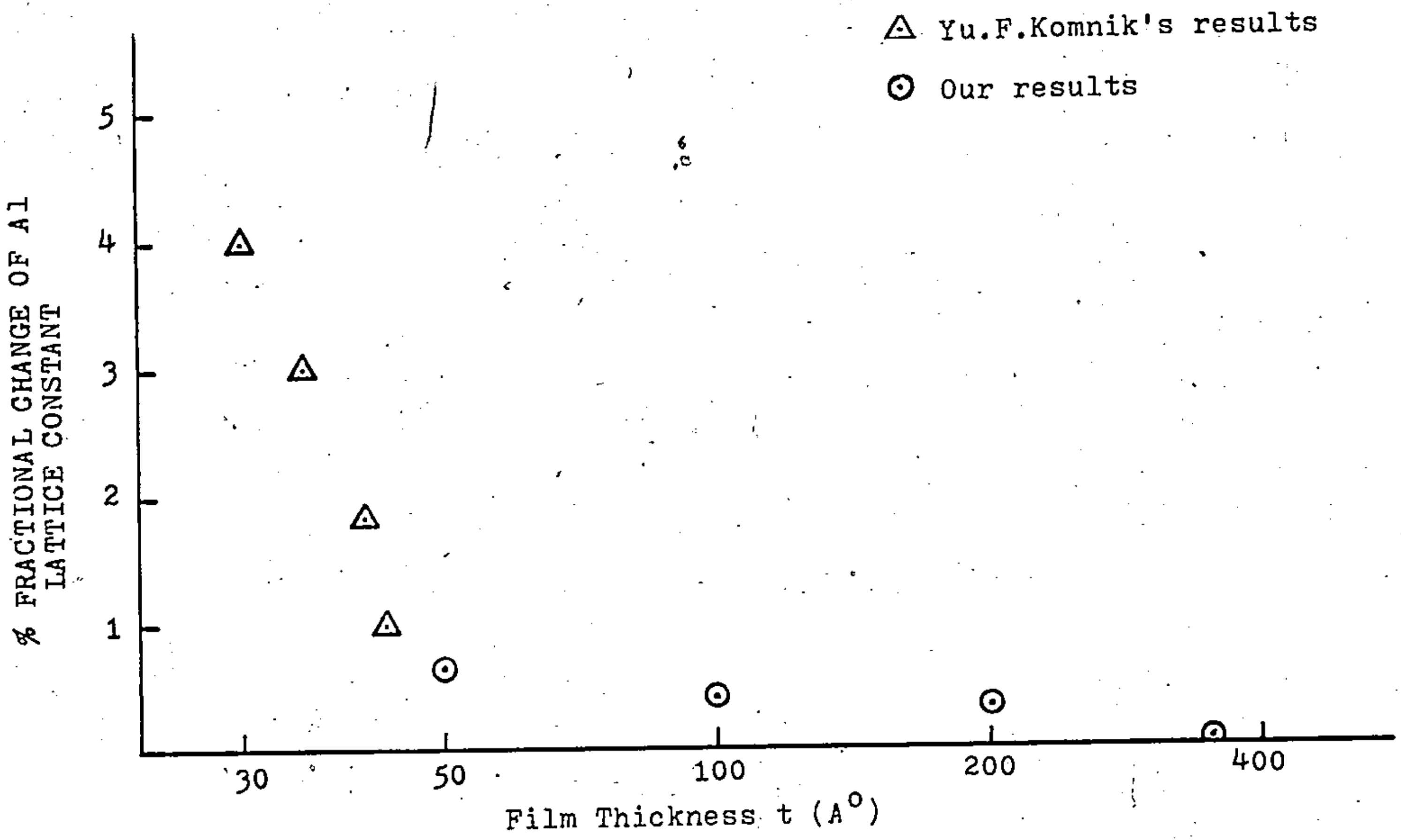

Fig. 6.1 Graph of %fractional change of Al lattice constant versus film thickness t .

As expected, the lattice constant changes abruptly as the film becomes discontinous.

The fact that the lattice constant of Al is found to increase with film thickness towards the bulk value indicates that thin Al films are subjected to pressures that do not exist in the bulk material. The sources of such pressures which result from various stresses in the film were discussed in chapter 3. It will be instructive at this point to investigate whether the variation of the lattice constant depends on the film thickness as observed experimentally, or if it is related to the size of the Al crystallites in the film. On such a basis the stress in the film might be one of two types;

(i) A stress acting throughout the whole specimen regarded as a thin elastic lamina.

(ii) a separate stress acting on each of the particles forming the specimen.

On the basis of the first hypothesis, we should expect the stress to depend on the thickness of the specimen, and to be greater for the thinner specimens. There would be no neccessary correlation between the magnitude of the stress and the crystallite size. The second hypothesis, on the other hand, would require that the magnitude of the stress should be inversely proportional to the size of the crystallites in the specimen. However, the size of the crystallites is not independent of the film thickness since it generally increases with film thickness.

The sources of the stress system (i) are:

__Thermal strains that films experience from the difference between the thermal expansion coefficients of the film and substrate when their temperature is changed.

__Lattice misfit as discussed in 3.2 (B) and

__compressive stresses arising from surface oxide layers.

Thermal strains can be easily calculated for the Al - TlCl system, but these represent only a few percent of the total strain involved in a thin film (20), (23) and so they can not account for the observed changes of the lattice constant on an individual basis. Interfacial dislocations and lattice misfits mainly occur in epitaxially deposited films, which is not the case for our vacuum evaporated Al films. Hence the contribution of this factor has been neglected. Surface oxide layers were not detected by electron diffraction. The presence of an amorphous oxide layer a few Angstroms thick is possible, but its interaction with the rest of the film would be too weak to account for any detectable changes of the lattice constant. Therefore one can safely arrive to the conclusion that stresses acting on the whole Al film, regarded as a thin lamina, can only account for a small percentage of the observed lattice contraction.

Stress system (ii) is the one applicable to polycrystalline materials. The major sources of stress here are surface tension of the individual crystallites, and grain boundary stresses. For discontinous film, surface tension alone can account for large volume contractions. Komnik's results (fig 6.1) show a 4% change for crystallites of 30A^{o} diameter, which reduces to 1% for 35A^{o} crystallites. This is just below the critical thickness for which the film becomes continous. Our results show a 0.6% change for films of critical thickness (50A^{o}), which reduces to 0.01% as the thickness increases to 350A^{o}. However, the case here is much more complicated than the one in discontinuous films. Surface stress alone exists only in the free surface; in the interior of a film we have a combination of surface stress, and grain boundary stress which we will call "intrinsic stress".

It is this mixture of stresses that produces the major volume contraction in thin Al films. Here we would like to propose a simple mechanism for the origin of the intrinsic stress. The proposal considers the film in the deposited state to contain a large amount of imperfections.
The term imperfections includes defects such as lattice vacancies, residual stresses resulting from bad thermal accommodation (low mobility) of the condensing material, and irregular crystallite boundaries.

Imperfections formed during depositions undergo change shortly after being trapped by succeeding layers of deposited metal. These changes take place at essentially the substrate temperature, perhaps with some help from the temperature pulses due to arriving atoms. Sufficient information to identify the imperfections with certainty is lacking at present. However, it seems likely that irregular regions on the growing surface, which become crystal boundaries when buried, rearrange and give rise to the principal part of the intrinsic stress through a reduction of volume. On the other hand, atomic migration might be sufficient to permit diffusion of vacancies to the free surface, which could introduce a further volume reduction. The intrinsic stress is then expected to vary with the substrate temperature. Increasing the substrate temperature should increase the surface mobility or arriving atoms and decrease the probability of attachment at an abnormal surface site. This should lead to a lower initial imperfection density and would reduce the intrinsic stress.

Summarizing the above, the lattice constant contractions are explained in terms of a mixture of surface stress and intrinsic stress acting on the individual crystallites of the film. The observed variation of the lattice constant with film thickness should therefore interpreted as a variation inversely proportional to the size of the Al crystallites.

6.2 Surface Stress Of Al Films Of Critical Thickness.

In films not containing intrinsic stress the average crystallite size can be determined with sufficient accuracy from the diffraction line broadening. Line broadening can in general be ascribed to lattice strains and / or small crystallite size. There is good evidence, however, that crystallite size is the predominant cause of line broadening for Al films of critical thickness (50A°).

As already mentioned, this evidence comes from the work of Rymer (50). According to Rymer the departure from a Gaussian curve for the intensity of a line indicates that line broadening is due to the effect of particle size. Such a departure would be manifested as a lack of linearity in a plot of log (I/Imax) versus $(\text{distance})^2$, if the distance from the line centre is considered such a departure was obtained from first order reflections of 50A° Al films. As it can be seen in figures 5.8 to 5.10 all line profiles deviate from a Gaussian form. The contours for the 111 and 220 line indicate that the broadening is due entirely to particle size,contour 200 shows that there is asmall amount of intrinsic stress involved in the broadening of the lines. Separation of the two types of broadening requires the study of second order reflections which unfortunately are not detectable with electron diffraction.

Assuming that the broadening due to intrinsic stress is negligible we can proceed to calculate the average diameter of the crystallites for the 50A^o Al films. Then the observed lattice contraction is interpreted in terms of the surface stress, T, according to the equation (45)

$$T = -\frac{3\Delta a\, D}{4\, a\, k} \qquad (6.1)$$

where Δa is the change in lattice constant of Al due to surface stress, a is the lattice constant for the bulk material D is the average diameter of the crystallites and $K=0.159\times10^{-11}\mathrm{cm}^2/\mathrm{dyn}$ is the compressibility coeficient. The average diameter of the crystallites can be calculated from the integral width, W_i of the diffraction rings using the relation (7, 35, 44, 52, 56)

$$D = R\,d/W_i \qquad (6.2)$$

where R is the radius of the diffraction ring and d, the corresponding plane spacing. The integral width is defined, as the area under the intensity curve divided by the maximum intensity.

* It should be noted here the compressibility coefficients of thin films could vary from the bulk value since they are subject to unusually high pressures. However, no specific information exists for Al thin films and the bulk value of K is used.

However, since I(x) is not known it can be approximated with the linear width W_1 which is the width of the line at half the maximum intensity. An assumption is made here that the measured value of W_1 is entirely due to crystallite size broadening, i.e: instrumental broadening is negligible. The average crystallite diameter D of the 50A° Al films was calculated from the linear widths of the 111, 200 and 220 reflections using equation 6.2 was found to be 56A°, subsequent use of equation 6.1 (a is given in table 4.1) gave a surface stress 1500 dyn/cm.

This value of surface stress, which corresponds to a 0.6% lattice contraction should be considered as a "fair" estimate, since a large number of approximations and assumptions are involved. However the obtained result is not unrealistic. The surface stress of silver fims below critical thickness with 0.7% lattice contraction was found to be 1415 dyn/cm (45); similarly a surface stress of 1175 dyn/cm was calculated for discontinous gold films (46).

PART TWO

APPARENT CHANGES IN THE LATTICE PARAMETERS OF INSULATING FILMS DUE TO SURFACE CHARGES

CHAPTER 7.

INTRODUCTION

In electron microscopy we often use thin non-conducting films of different kinds. One kind of non-conducting film is a supporting film, such as collodion and formvar, which are widely used because of simple preparation. Other electrically non-conducting films are insulating object films such as CaF_2, ZnS, NaF, TlCl etc.

Bombardment of such specimens with electrons can result in the accumulation of electric charges on them. This produces unfavourable effects, such as reduction of resolution and change of the angle of diffraction so as to produce a change in the diameters of the diffraction rings. These effects become evident in a rather disturbing way in reflection and interference microscopy, however they are not entirely undetectable in transmission microscopy.

The aim of this work is to investigate evidence for the existence of these charges and to estimate the order of magnitude of the above mentioned effects. During the course of observations on insulating thin films such as formvar, TlCl, NaF, LiF and CaF_2 we have managed to detect the existence of fluctuating charges on these films using "shadow" electron microscopy. The observed phenomenon appears as a flickering pattern whose appearance is suggestive of a "bee swarm".Such patterns did not appear in conductive films of Al, Au and carbon support films.

CHAPTER 8.

IMAGING OF FLUCTUATING CHARGES BY SHADOW PROJECTION.

8.1 Introduction:

Shadow projection is an electron optical method of viewing effects produced by electric and magnetic fields. The method was developed by L.Marton (66). M.E. Hale(67) first demonstrated the use of the method for the observation of domain walls in thin ferromagnetic films. H.Mahl(68) observed the fluctuating granularity or "Bee Swarm" effect which is produced by the presence of electric fields in thin insulating films.

For such observations a standard transmission electron microscope can be employed. In this chapter, the theory of shadow projection and the modes of operation of the electron microscope will be examined.

8.2 First Order Optics:

The shadow method is theoretically applicable to the quantitative evaluation of a wide variety of electric and magnetic fields. The formulas that will be derived are based on relations between field distribution, electron deflection, and the geometrical parameters of the focusing system.

The electron optical arrangment used for obtaining images of the effects produced by the deflecting fields is shown schematically in Fig. 8.1 The deflecting field is placed in the vicinity of the point Q and for simplicity is assumed so oriented that trajectories incident in the plane of the figure remain in that plane after deflection.

A converging lens is placed at some distance L from Q outside the deflecting field. In the absence of the field, a parallel incident beam of electrons (dashed rays U,U+) will converge to the focus of the lens F, whose principal planes are P, P' and then diverge past a thin obstruction GG+ which will cast a shadow NN+ on the screen S.

When a deflecting field is placed at Q a different pair of rays (solid rays D,D+) will determine the shadow boundary of the obstruction G,G+. The focus F will then be displaced to some point E, and the resulting displacement of the shadow NN+ to AA+ can be measured and substituted into theoretical formulas to obtain an estimate of the field strength. It can be shown (67) that the general key equation for the determination of field strength is

$$a - rg - (r - 1)f\phi' = 0 \qquad (8.1)$$

where: a = distance SA

r = NN+ / GG+

= magnification of obstruction GG+ as determined by its shadow on screen in the absence of the deflecting field.

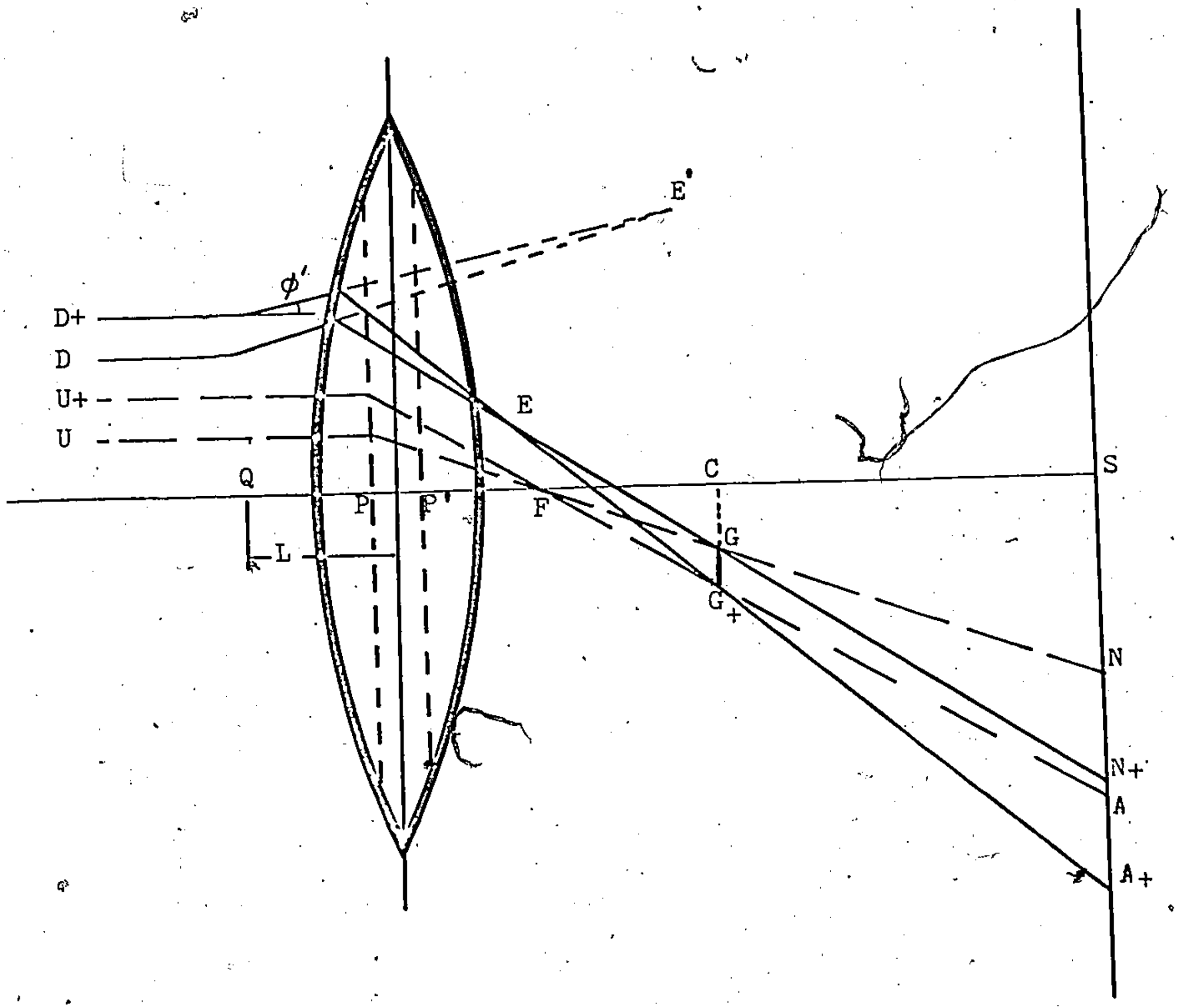

Fig. 8.1 Electron optical diagram of the shadow projection method of mapping of electromagnetic fields.

ϕ' = deflection angle of ray DGA

g = distance CG as shown in the diagram

f = focal length of the lens

The above formula is valid for systems that have the following properties:

(a) All lateral distances and angles measured from the optical axis, are sufficiently small to make geometrical aberrations negligible.

(b) The distance between the deflecting field and the field of the lens is sufficiently great so that the interaction between the two fields may be neglected.

(c) The accelerating potential of the electrons is not in relativistic range.

The next step is to calculate the deflection ϕ' as a function of the field distribution parameters. Hence on substitution of such a function for ϕ', one obtains from equation (8.1) a relation between the unknown parameters of the deflecting field and known parameters of the apparatus.

8.3 Electron Deflection And Field Strength:

Figure 8.2 shows a typical electron path y = y(x) through the deflecting field to be studied. The x axis is taken to coincide with the optical axis of the system. The incident asymptote is parallel to the x axis and characterized by b'. The emerging asymptote is characterized

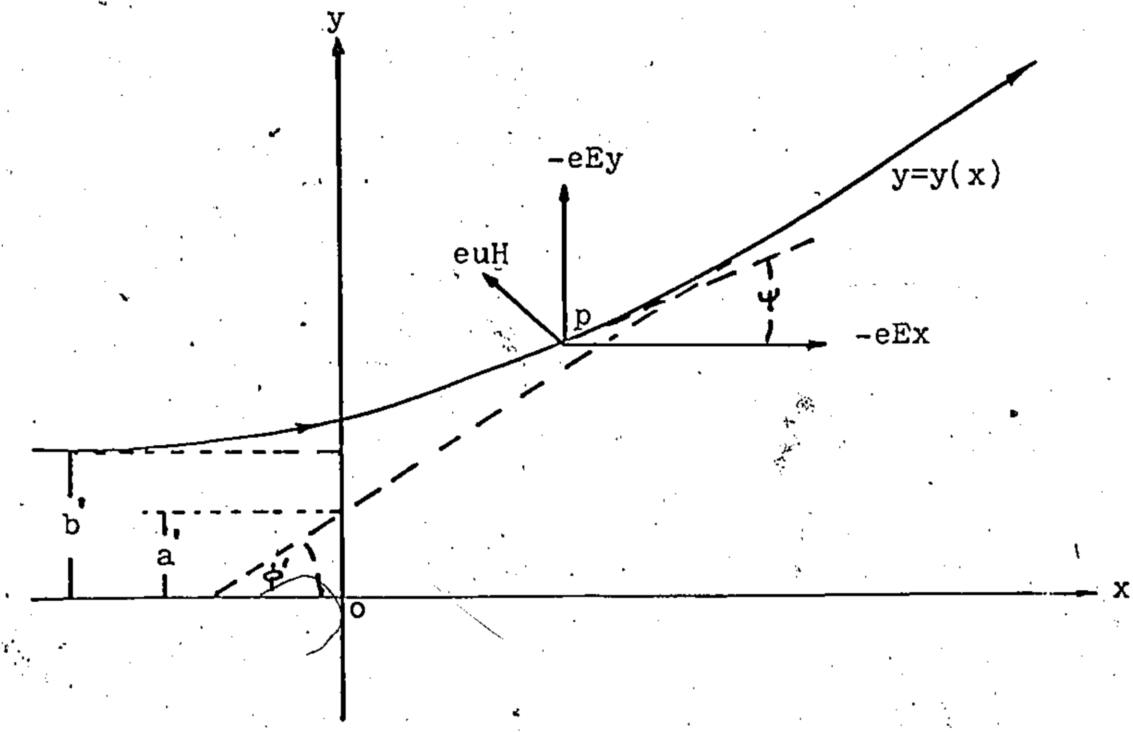

Fig. 8.2 Coordinate diagram of typical plane electron trajectory in deflecting field.

by slope tan ϕ' and the intersection with the y axis a'. The components $E_x(x,y)$ and $E_y(x,y)$ of the electric field are in the plane of figure 8.2 and the magnetic field vector H(x,y) is directed normal to this plane.

If the direction of the vector H(x,y) is defined as positive when directed upward from the plane, the normal force F(x,y) on the electron at any point (x,y) of the trajectory is

$$F(x,y) = e(E_x \sin\psi - E_y \cos\psi + uH) \quad . \qquad (8.2)$$

where e, m and u are the charge, mass and velocity of the electron respectively, and

$$\tan\psi(x,y) = \frac{dy}{dx} \qquad (8.3)$$

is the slope of the trajectory at a point P(x,y).

If V(x,y) is the accelerating potential of the electrons, and condition (c) of the previous section is taken into account then

$$E_x = -\frac{\partial V}{\partial x} \;, \quad E_y = -\frac{\partial V}{\partial x} \;, \quad u = \left(\frac{2eV}{m}\right)^{\frac{1}{2}} \qquad (8.4)$$

From the curvature of the trajectory 1/R(x,y) at a point (x,y) we have

$$\frac{d^2y}{dx^2}\left[1 + \left(\frac{dy}{dx}\right)^2\right]^{-\frac{3}{2}} = \frac{1}{R(x,y)} = \frac{F(x,y)}{mu^2} \qquad (8.5)$$

substituting 8.2, 8.3 and 8.4 into 8.5 one obtains a differential equation for the trajectory y = y(x)

$$\frac{d^2y}{dx^2}\left[1+\left(\frac{dy}{dx}\right)^2\right]^{-\frac{3}{2}} -(e/2mV)\; H+\left[\left(\frac{\partial V}{\partial x}\right)\frac{dy}{dx}-\frac{\partial V}{\partial y}\right]+\left[\left(\frac{\partial y}{\partial x}\right)^2\right]^{-\frac{1}{2}}/2V=0 \qquad (8.6)$$

but condition (a) of the last section implies

$$\frac{dy}{dx} \ll 1$$

therefore equation (6) becomes

$$y''(x)+\left[\left(\frac{\partial V}{\partial x}\right)/2v\right]y'(x)-\left[\left(\frac{\partial V}{\partial y}\right)/2V+(e/2mV)^{\frac{1}{2}}\,H\right]=0 \qquad (8.7)$$

equation 8.7 is the equation that relates the deflection ϕ' with the deflecting fields. When analytical expressions are substituted for V(x,y) and H(x,y) in equation 8.7 the deflection ϕ' can be calculated as a function of V(x,y) and or

H(x,y).

8.4 Uniform Electrostatic Field.

As an application of the previous theory we will consider a simple way of estimating the "effective lateral deflecting field" in thin insulating films. The deflecting field is that of two parallel plates separated by a distance 2D, and at potentials Vo + ΔV, Vo - ΔV, where Vo is the potential corresponding to the initial energy of the electron beam. The plates are placed parallel to the optical axis (parallel to plane xz fig 8.2), with the origin O at the field centre, their dimension being 2Xo. Since the field between the plates is uniform we have

$$\frac{\partial V}{\partial y} \equiv \frac{\Delta V}{D} \;, \qquad \frac{\partial V}{\partial x} = 0$$

substituting the above information in equation 8.7 we find an expression for the angle of deflection of an electron incident parallel to such plates.

$$y'(x) = \frac{X \Delta V}{V D} = \tan \phi' \sim \phi'$$

This is the well known formula for a parallel plate capacitor. The quanities ϕ', V_o and X_o are known or measurable parameters thus the deflecting field V/D may be calculated.

CHAPTER 9.

EXPERIMENTAL RESULTS AND DISCUSSION.

9.1 Observations By Shadow Microscopy

In shadow projection of a thin insulating film, when using sufficiently narrow aperture of the electron beam emitted from the source, one can observe a fluctuation of bright points on the screen resembling a "bee swarm". This phenomenom is observed at low magnifications by means of a viewer.
If the angular aperture of illumination is increased, a certain value is reached for which the fluctuating charges become bright points, loose their contrast with respect to the background and cease to be perceptible. At this point the angular aperture of the electron beam reaching the specimen is greater than the angular deflections caused by the charges.

Figures 9.1 and 9.2 show micrographs of a formvar support film under bright field and shadow microscopy. The exposure time was as low as possible since the fluctuating charges are in constant motion. The life time of the flickering spots was estimated to be much less than a second. However, the shortest exposure time was of thr order of a few seconds, hence Fig 9.2 shows a time average picture of the effect.

The size of each granule was found to be approximately 0.5 μm. Similar observations have been made by T.Komoda and S.Hosoki (69). These workers have observed the "bee swarm" effect

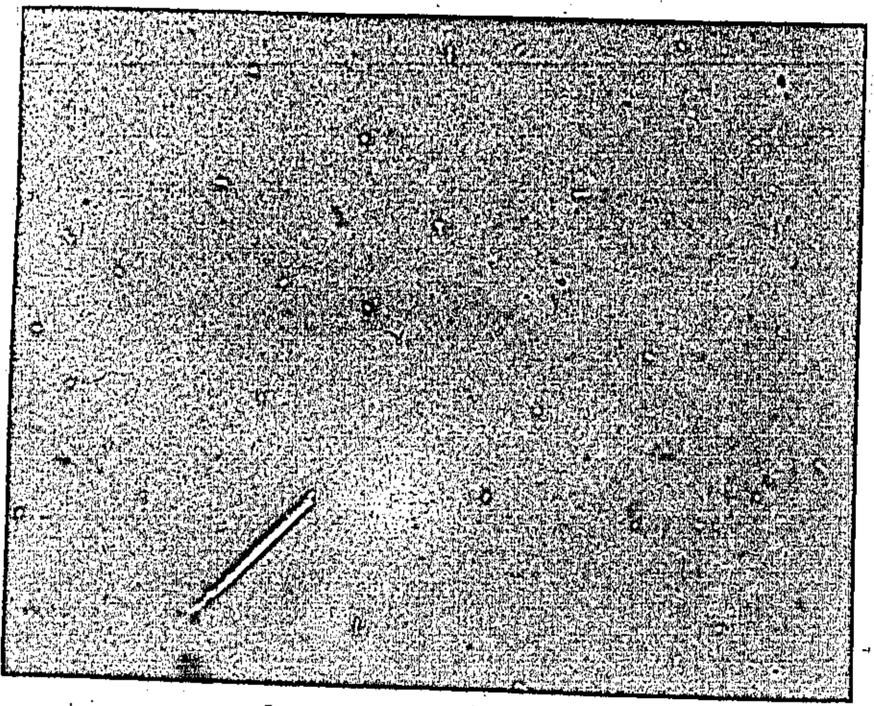

Fig. 9.1 Bright field micrograph of a formvar support film. Magnification: 1:2500

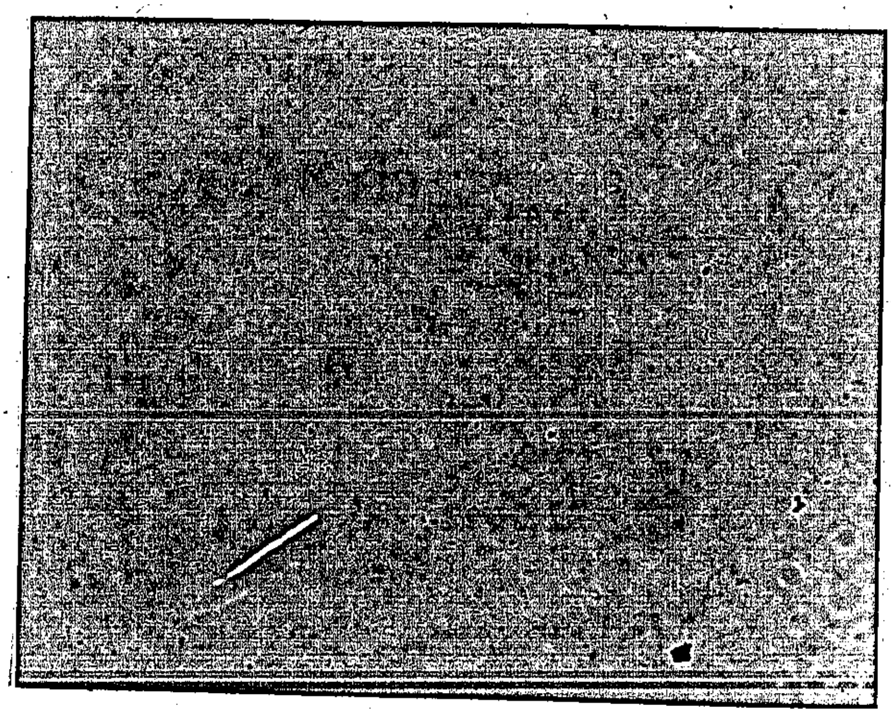

Fig.9.2 Shadow projection micrograph of the above formvar film.

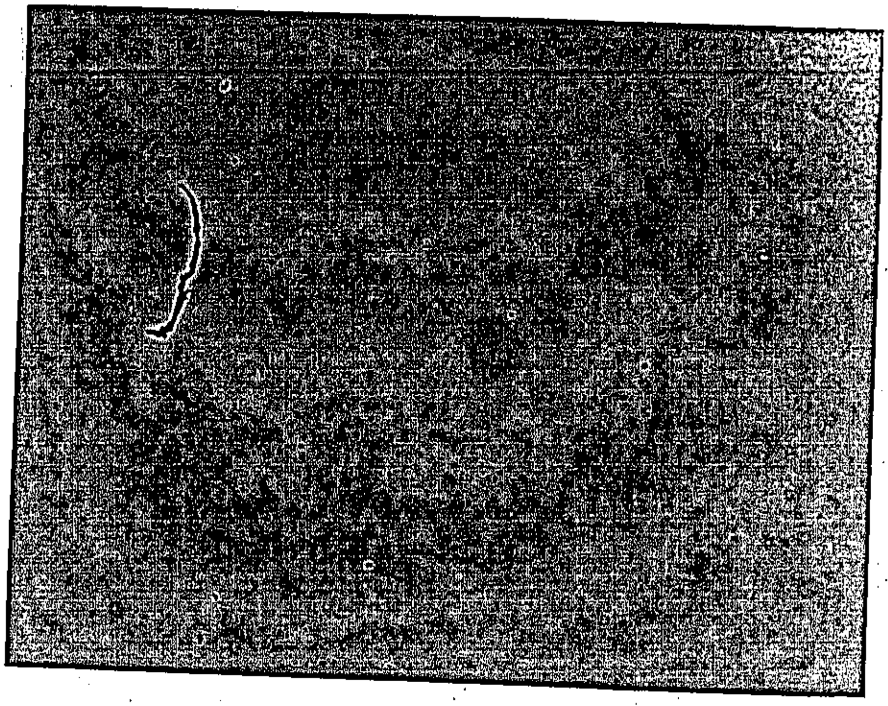

Fig. 9.3 Bright field micrograph of a 300 A° CaF_2 film Magnification, 1:5000

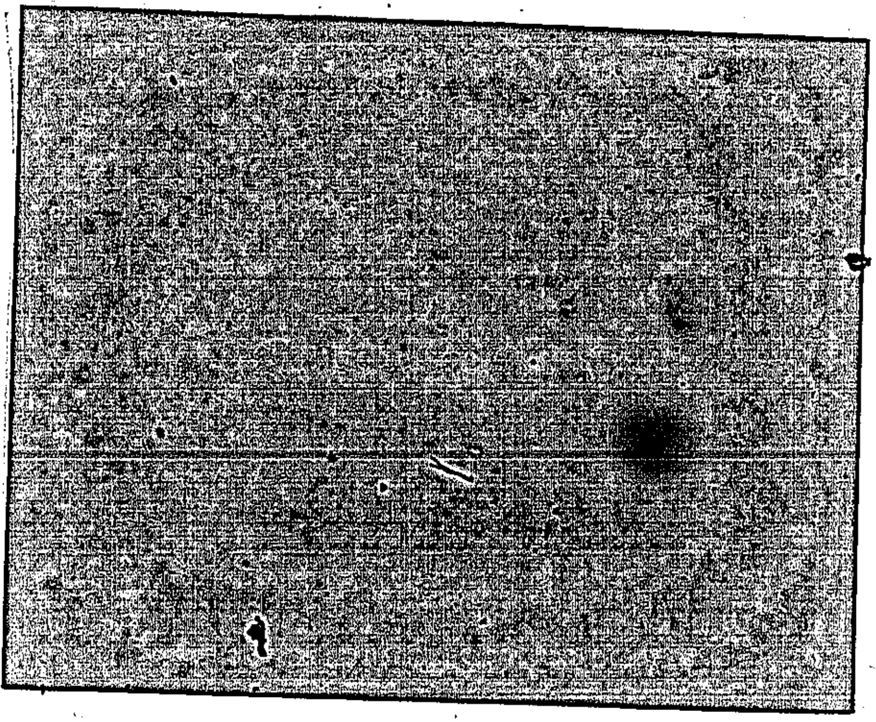

Fig. 9.4 Shadow projection micrograph of the above CaF_2 film.

using an intensifier and cine camera. They found that the mean lifetime of a flickering spot is about 0.1 second, and that the mean granule size is 0.2 - 0.4 m. Figures 9.3 and 9.4 show similar observations for a CaF_2 film.

Two modes of operation of the electron microscope were investigated, one using projector magnification alone, and one using both objective and projector lenses. These modes were suggested by H.W. Fuller and M.E. Hale (70), for the observation of domain walls in thin ferromagnetic films. Our results on electrostatic fields in insulating films show that the properties of the two modes are the same as these of magnetic fields in ferromagnetic films. Our results show that the two modes are also capable of showing electrostatic fields in insulating films.

9.1.1 Mode A.

Mode A is shown in Fig 9.5. Figure 9.7, shows an electron micrograph of the "bee swarm" effect in a formvar support film using mode A. In this mode of operation of the electron microscope the principal features are:

(a) Extreme overfocusing of the condenser to give a small, distant, effective illuminating source.

(b) Objective lens off.

(c) Intermediate lens off.

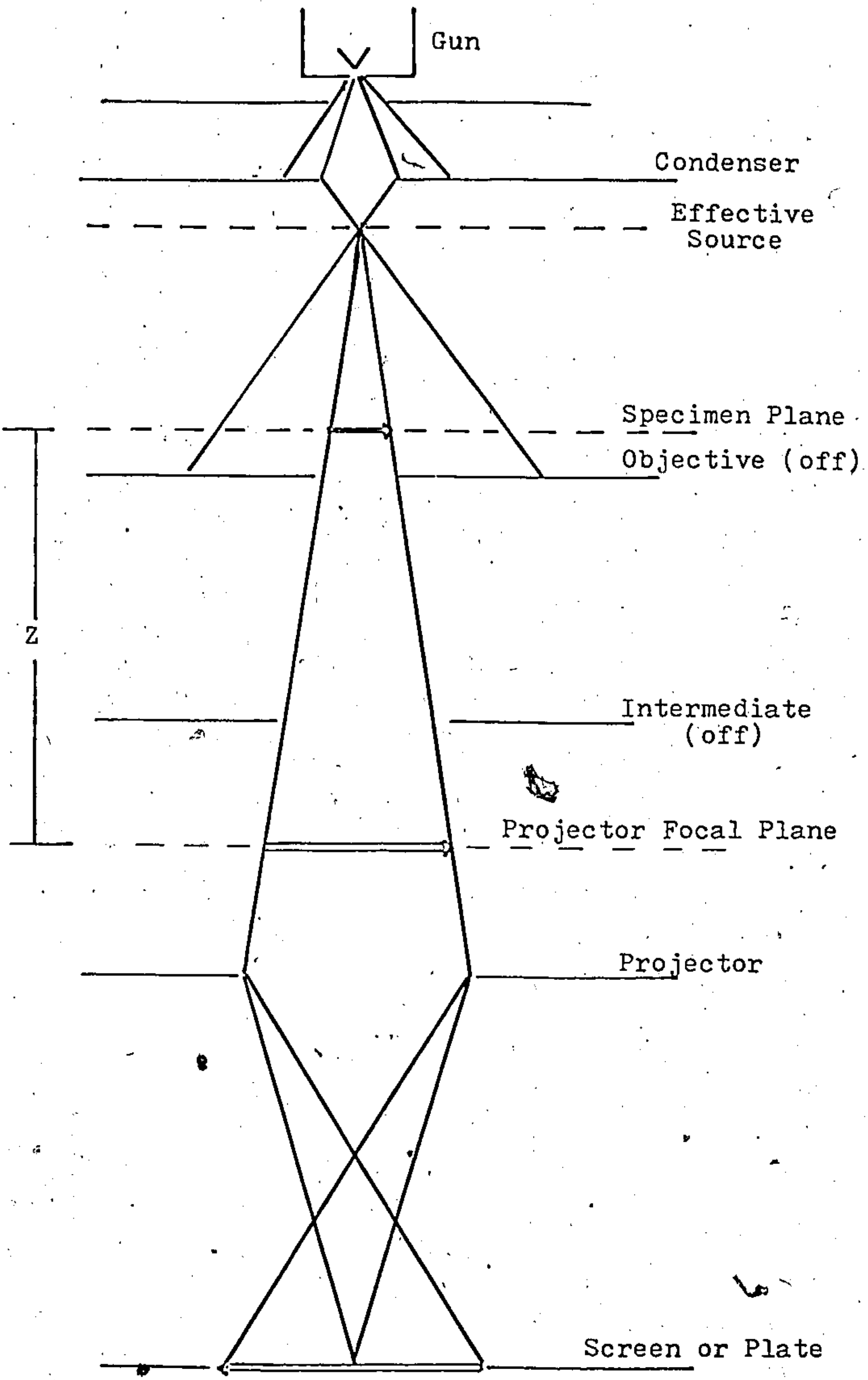

Fig. 9.5 Ray diagram of "mode A" for imaging fluctuating charges on the specimen.

Then a shadow image of the specimen appears in the focal plane of the projector lens at distance Z below the specimen. This image is magnified by the projector lens and projected into the fluorescent screen.

The magnification of the projector lens can be controlled either by manual control of the lens currents (i.e. microscope on "free") or by setting the microscope on "Zoom" and varying magnification control. The latter method is simpler and free of lens abberations that can be produced by bad combination of the lens currents when controlled manually.

A modification of mode A is to keep the intermediate lens "ON" and turn off only the objective. In this manner the overall magnification is reduced without changing the projector current.

Mode A provides high magnification of the shadow image (i.e. with respect to mode B) and in the case of electrostatic deflecting fields the primary advantage is the great sensitivity.

9.2.2 Mode B.

A second mode of operation of the electron microscope is shown, schematically in fig.9.6 where the objective is operated at reduced strength to focus a virtual object plane (which results at a distance Z above the specimen), on the projector focal plane. The remaining conditions are the same as in mode A

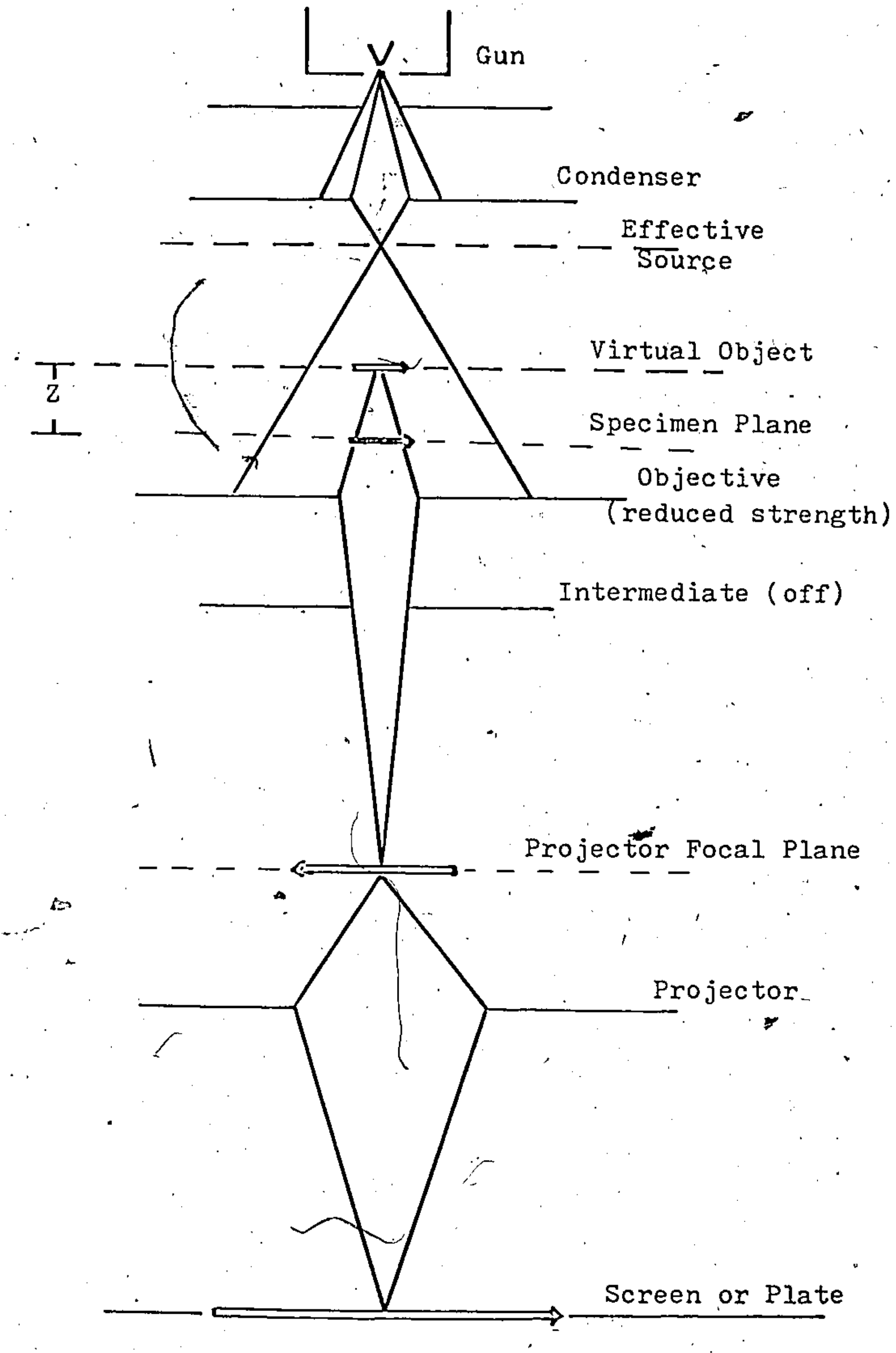

Fig. 9.6 Ray diagram of "mode B", operation for high resolution and magnification of charge images using objective and projector lenses.

except that the lens currents can only be controlled manually. In this manner the ammount Z of defocussing can be arbitraily adjused away from zero. A shadow projection of the specimen of fig 9.7 by mode B is shown in fig 9.8.

This particular operation results in a much higher resolution than that of mode A. In the presence of an electric deflecting field, the improvement in resolution results from an increase in contrast.

So we observe that both modes A and B produce a defocusing Z which is neccessary for the imaging of the charges on the specimen. Note that at focus (i.e. Z = 0) the electron deflection s caused by the charging of the specimen do not result in the "bee swarm" effect. This is because the electrostatic angular deflections are well within the angular aperture of the objective lens, and as for any scattering mechanism in this event, the deflected electrons are returned to the correct point in the image plane.

For better comparison of the two modes of operation a section from fig 9.7 and fig 9.8 are blown up in Figures 9.9 (a) and (b) respectively.

Fig 9.7 shadow projection micrograph of a formvar support film operating the microscope in mode A.

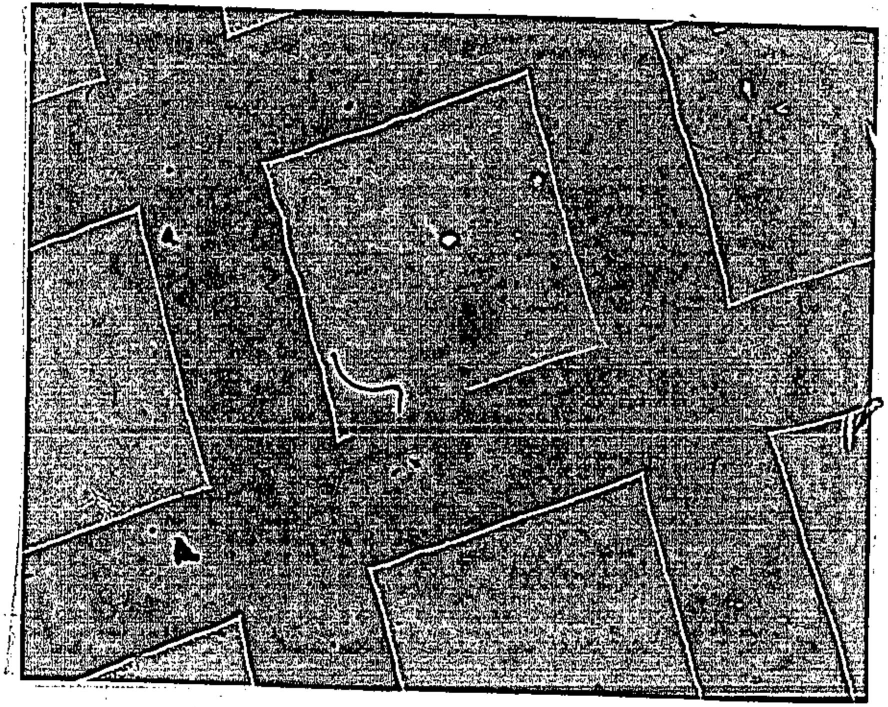

Fig 9.8 Shadow projection micrograph of the same formvar film as in fig. 9.7 operating the microscope in mode B.

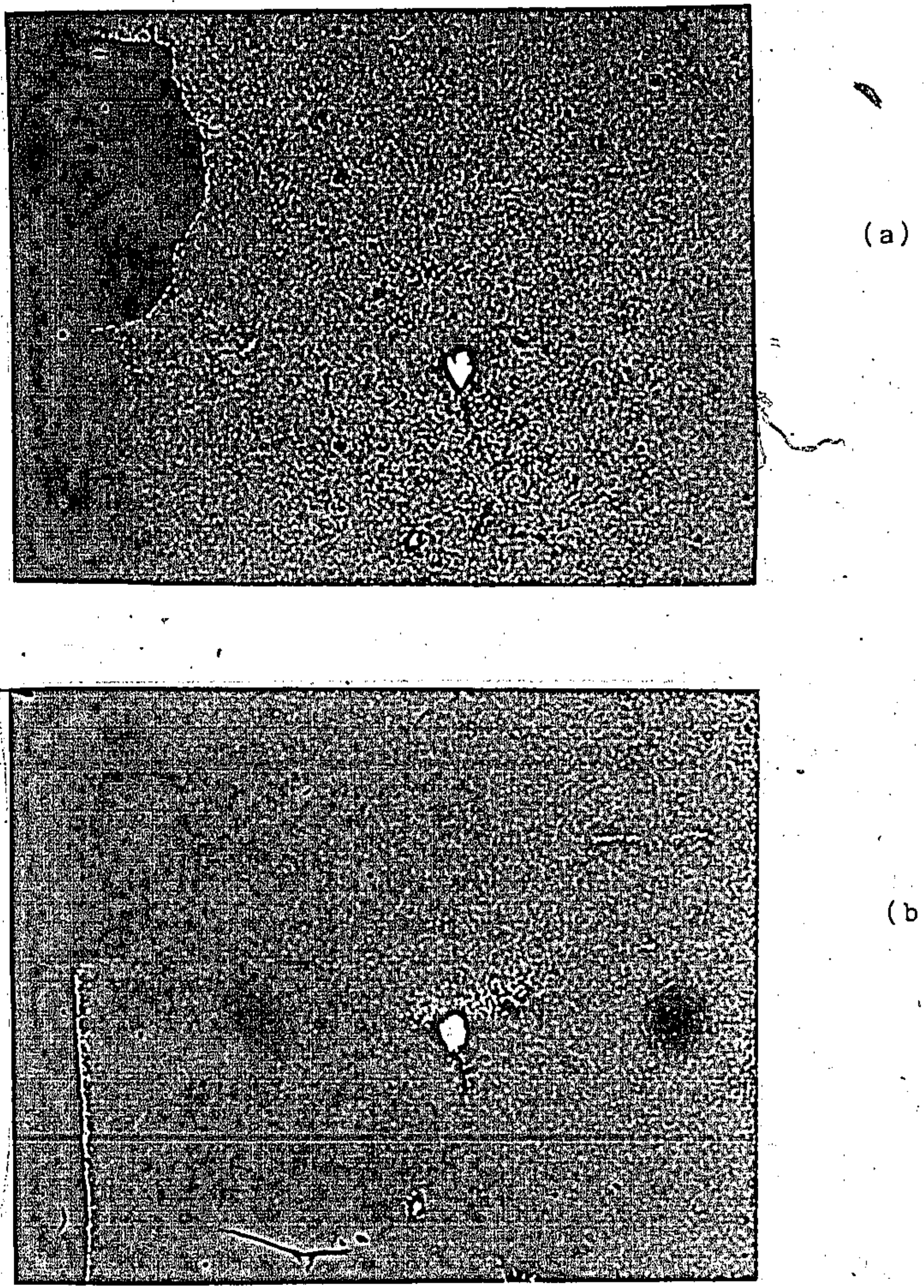

Fig. 9.9 (a) Enlarged section of fig. 9.7,operation mode A.
(b) Enlarged section of fig. 9.8,operation mode B.

9.2 Deflection of the Diffracted Beam caused by Specimen Charge.

It the specimen acquires an electric charge, we should expect a change in the diffraction angle so as to produce a change in the scale of the diffraction pettern. Hence measurement of the diffraction pattern of the charged specimen and comparison with the diffraction pattern of the uncharged specimen will reveal the change in the angle of diffraction. Since any insulating film will charge up when bombarded with an electron beam, a discharging of the film is needed in order to obtain the diffraction pattern of the uncharged specimen. The discharging can be done by the use of a special attachment to the electron microscope, which consists of an electron gun emitting low energy electrons which neutralize the specimen. However, we employed a method which is much simpler and equally effective. When selecting the area of diffraction on the specimen, part of the copper grid is included in the illuminating area. The copper grid bar emits sufficient secondaries to discharge the surrounding regions of the specimen. Further evidence of such discharging is given by G.H. Curtis and R.P. Ferrier ('71). These workers showed that when the grid bar is not included in the irradiated area of the specimen, the part which is exposed to the beam charges up to such an extent that it forms a converging electrostatic lens. Under such conditions the image "explodes" to one of much higher magnification. When the grid bar is included in the illuminated area this effect was very much smaller.

Insulating films of NaF, Lif and CaF_2 200 A^o thick where studied. For each specimen two diffraction patterns were taken in quick succession, one including the copper grid bar in the illuminating area (discharged) and one without (charged). The accelerating pottential was set at 100KV. The measured ring diameters of the charged and discharged specimen for a number of reflections is shown in tables 7 - 9. For each specimen, a graph of the difference in the charged and discharged diameters versus the corresponding reflection (hkl) is plotted in figures 9.9 - 9.13 . We observed that within the experimental error a straight line can be drawn through the points as it was expected. That is the ring diameters of different reflections change by the same amount ΔD.

The change in the diffraction angle can now be found from ΔD and the camera length L, which is calculated from equation 4.1. The results of the calculations are shown in table 6.

Table 6.

Specimen	D (μm)	ϕ' (rad)
LiF	120 ± 35	7.5×10^{-5}
NaF	20 ± 35	1.2×10^{-5}
CaF_2	35 ± 35	2.2×10^{-5}

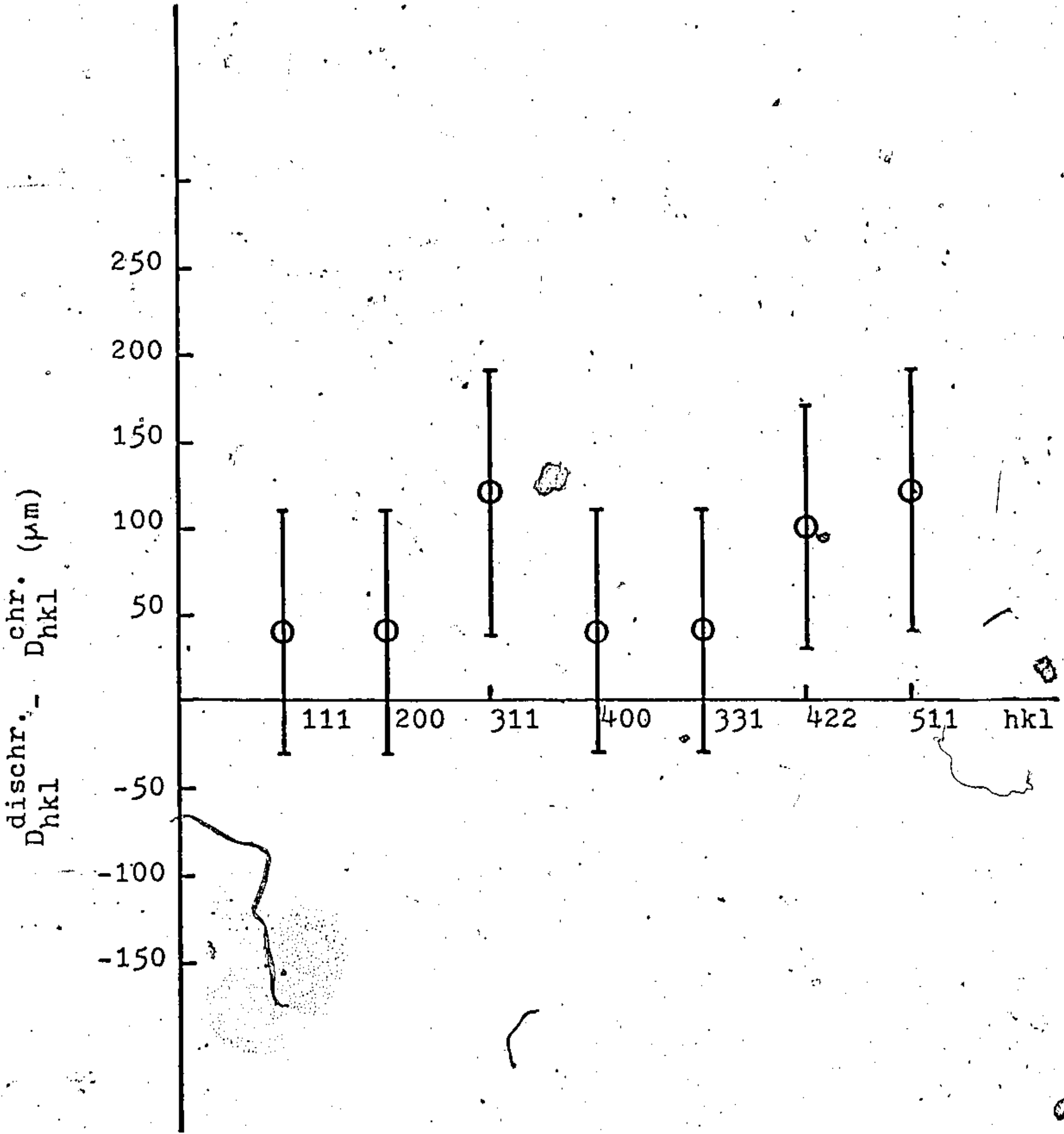

Fig. 9.10 Difference in the charged and discharged diameters of a CaF_2 film for various reflections.

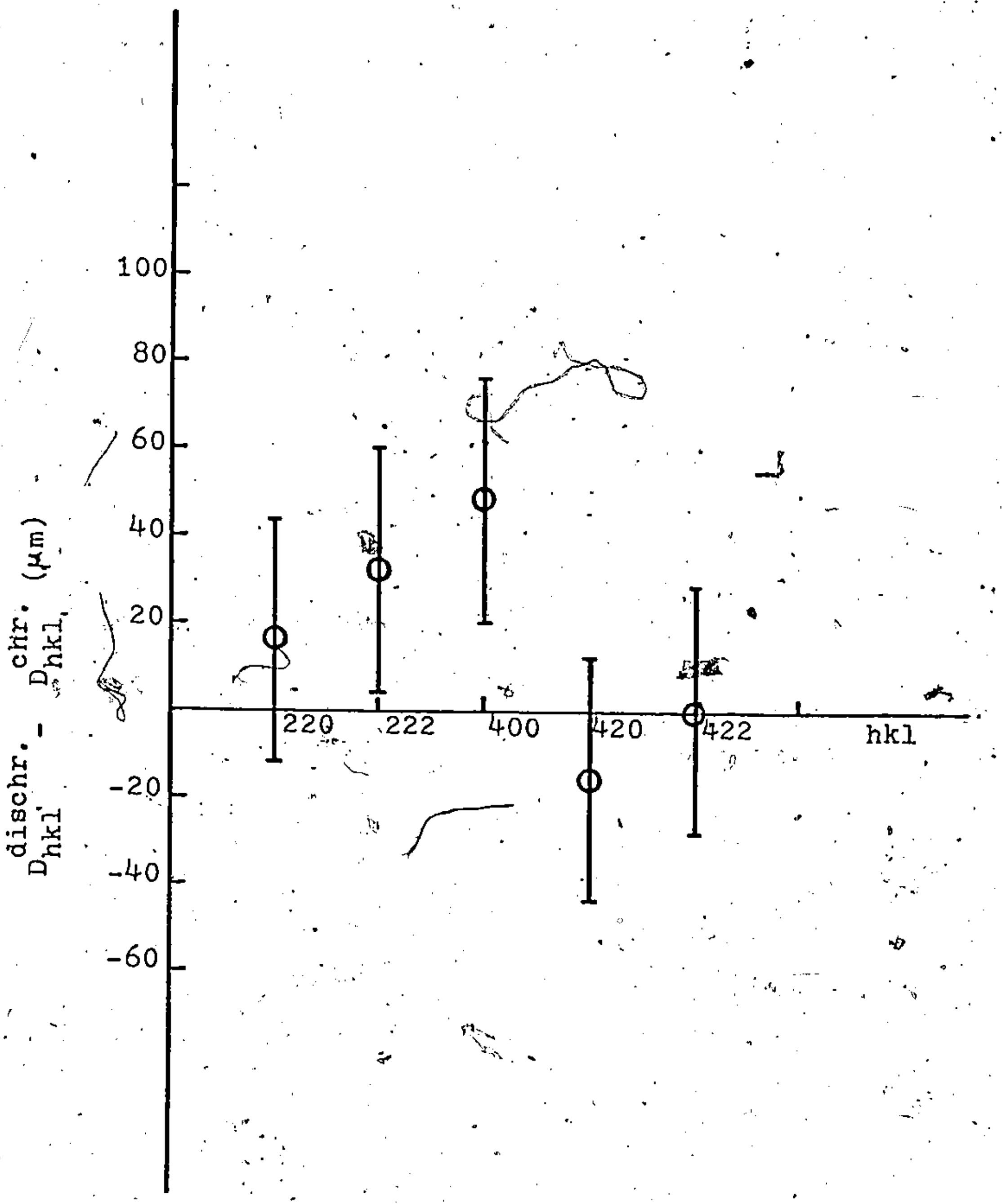

Fig. 9.11 Difference in the charged and discharged diameters of a NaF film for various reflections.

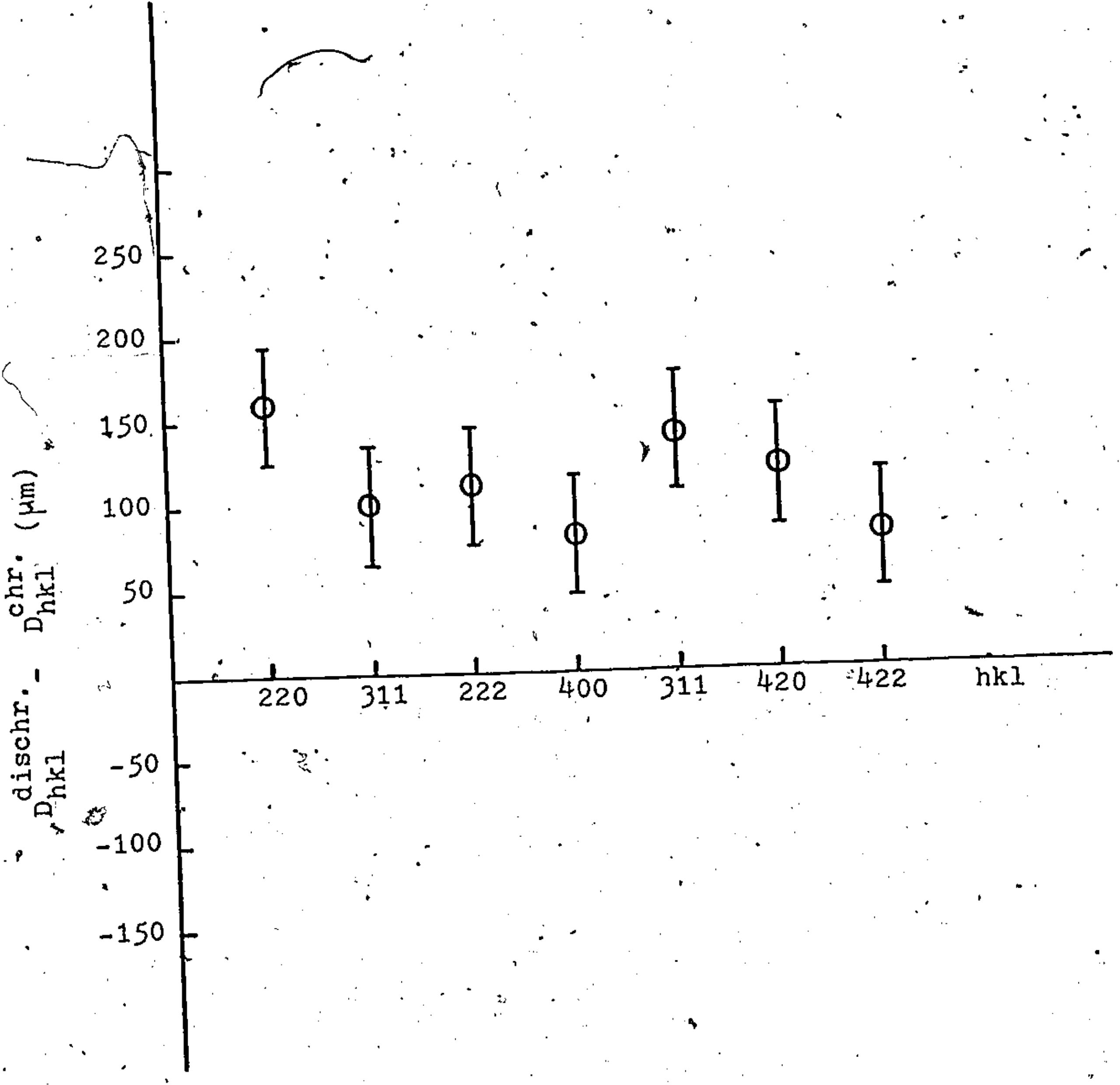

Fig. 9.12 Diference in the charged and discharged diameters of a LiF film for various reflections.

We note that the omission of the copper grid from the illuminating area resulted in a reduction of the ratio of the diffraction pattern, this corresponds to positive charge on the specimen. However, the error in the calculation of ΔD is relatively large, and the only conclusive indication that the charged D_{hkl} are smaller than the discharged D_{hkl} is given from the LiF results. Considering only the LiF results, $\Delta D=120 \pm 35 \mu m$ represents at least a +0.2% "apparent" change in the lattice constant of the charged LiF films. Hence if the specimen is not discharged therecould be false indications about the structure of the LiF films, or any other non conducting films. However, the magnitude of the change is open to question, for, the structure of the film close to the grid could be slightly different from that of the rest of the film. This argument is based on observations of the structure of the films close to the grid bars. Sometimes it appears to be different from the rest of the film, and very often cracks appear on the film around the grid boundaries. A possible explanation of these observations could be the difference in the thermal expansion coefficient and the rigidity of the formvar in contact with the grid, and that suspended in between the bars.

The values of the deflection angle $\emptyset'$ compare well with previous measurements that employed different experimental methods. Drahos and Delong (72) reported a deflection angle

Ø' = 5 μrad, for 75 Kev electrons calculated from absolute measurements of the optical system equation 8.1. H Mahl (68) estimated the value of Ø' around 10 μrad for 40 Kev electrons, this estimation was also based on measurements of the optical system. Finaly Komoda and Hosoki using an image intensifier reported a value of Ø'=100 μrad for 100 kev electrons.

The observed deflection of the electrons imply the existence of a deflecting field, the strength of which is of importance since it could be related to dielectric break down of thin insulating films under electron bombardment.

9.3 Field Strength and Mechanism of the "Bee Swarm" Effect.

The effect of the presence of electric fields on insulating (non conducting) thin films have already been discused by some authors. Mahl and Weitsch(68) using the approximation that the electric fields involved are effective only within the thickness of the specimen, calculated the field strength to be about 100MVm^{-1}. Dove (73) however considered the extension of the microfields extend into space on each side of the film, over an effective distance equal to the average diameter of the the fluctuating spots. In this manner he calculated a field strength of 800kVm^{-1}. Komoda and Hosoki also reported a value of $100 MVm^{-1}$. A different approach was made by Curtis and Ferrier (71). They assumed that most of the generated charge resides in the surface of the film so that the thickness of the film is almost irrelevant. Thus they considered the external fields entirely responsible for the deflections of the electrons. They derived the folowing equation for the maximum field strength.

$$E = \frac{2\pi}{g'} \varnothing' U \qquad (9.1)$$

where g' is the size of the flickering spots, $\varnothing'$ the deflection angle and U the accelerating potential. Substituting our experimental results into this expression, that is the mean granule size $g'=0.5\ \mu m$ and the angular deflections ranging aproximately from 10^{-5}-10^{-4} rad at 100kv, the maximum field strength becomes $E \simeq 10\text{-}100 MVm^{-1}$. This value of E compares well with the ones mentioned above.

The following mechanism is proposed for the "bee swarm" effect. The formation of the electostatic fields in general will be expected to depend upon factors such as beam and film geometry, secondary emission ratio, stopping power, and micro- and macroscopic properties such as resistivity and polarizability. The accelerated electrons on passing through the specimen eject from it secondary electrons, some of which ground themselves by moving to the grid, and the rest of which return to the specimen.

For small values of E the escaped electrons are replaced with others drawn into the specimen via the space charge of the emitted secondaries. For larger values of E such as the ones obtained here, another process may start which mey be described as surface dielectric breakdown. Positively charged regions form which the charge builds up to a critical value (size of the flickering spots) and then discharges. That is, the observed "bee swarm" effect is a charge - discharge process on the film surface. This is possible since the fields required for, dielectric breakdown of plastic materials are of the order of 10 - 20 MVm^{-1}, and this figure lies in the range of the calculated field strength. There is also evidence (74) that many results obtained in studies of insulator surface breakdown can be explained in terms of surface charges.

Table 7. Measured electron diffraction ring diameters D_{hkl} of the charged and discharged CaF_2 film.

Reflection hkl	D_{hkl} charged (cm)	D_{hkl} discharged (cm)	$D_{hkl}^{dischrd.} - D_{hkl}^{chrd.}$ (μm)
111	1.688	1.690	20
220	2.762	2.764	20
311	3.236	3.242	60
400	3.908	3.910	20
331	4.264	4.266	20
422	4.792	4.796	40
511	5.078	5.084	60

Table 8. Measured electron diffraction ring diameters D_{hkl} of the charged and discharged LiF film.

Reflection hkl	D_{hkl} charged (cm)	D_{hkl} discharged (cm)	$D_{hkl}^{dischrd.} - D_{hkl}^{chrd.}$ (μm)
220	2.184	2.200	160
311	2.572	2.582	100
222	2.678	2.690	120
400	3.094	3.102	80
311	3.384	3.398	140
420	3.472	3.480	120
422	3.808	3.816	80

Table 9. Measured electron diffraction ring diameters D_{hkl} of the charged and discharged NaF film.

Reflection hkl	D_{hkl} charged (cm)	D_{hkl} discharged (cm)	$D_{hkl}^{dischrd.} - D_{hkl}^{chrd.}$ (μm)
220	1.964	1.966	20
222	2.410	2.414	40
400	2.787	2.592	60
420	3.122	3.120	20
422	3.418	3.418	0

CHAPTER 10

CONCLUSION

In spite of the various limitations in our experimental conditions, the present study was able to yield meaningful results. With an internal standard of vacuum deposited thallium chloride, the lattice constant of Al films were determined using the SAD technique to within an error of less than 0.1%. The lattice constant of Al was found to decrease from the bulk with film thickness. The lattice parameter contractions ranging from 0.6% to 0.01% of bulk value were observed for film thicknesses ranging from 50 - 350A° respectively. The lattice contractions were found to depend on a surface stress and an intrinsic stress acting on the individual crystallites of the Al films. The formvar diffraction pattern and its contribution to the background intensity was investigated. It was shown that there are three broad diffraction rings which should be taken into consideration when the line profiles or broad specimen rings are studied.

Investigation of the line broadening of 50A° Al films indicated that in films of this thickness, broadening due to particle size is the dominant factor. Under the assumption that the intrinsic stress is relatively small surface stress of 1500 dyn/cm was found responsible for the major part of the observed lattice contractions. The value of this stress should be considered as an order of magnitude since a number of assumptions were involved in its calculation .

The charges on surfaces of insulating films were detected by shadow projection microscopy. Both of the investigated modes of operation of the electron microscope for the imaging of the charges were found satisfactory. The same arrangement of the optical system as given in this paper, can be employed for the observation of magnetic domains in thin ferromagnetic films. The nature of the surface charges and the resulting electrostatic fields was studied in an indirect manner, by measuring the angle of diffraction of the electron beam. Deflections up to 100µrad (for LiF films) were obtained, corresponding to a deflecting field of 100 MVm^{-1} and a 0.2% apparent change in the lattice constant of the specimen. The "bee swarm" effect was explained as a two process mechanism, that is exchange of electrons with a space charge cloud near the film, and surface dielectric breakdown.

REFERENCES

1. J.E. Lennard Jones and B.M.Dent. Proc. Roy. Soc. A121, p.247 (1928)
2. M.M. Nicolson. Proc. Roy. Soc.A228, p.490 (1955)
3. R. Shuttleworth. Phys. Soc.A63, p.444 (1950)
4. G.I. Finch and S.Fordham. Proc. Phys. Soc. 48, p.85 (1936)
5. H. Boochs. Ann. Physics. 35, p.333 (1939)
6. E. Pickup. Nature London. 137,p.1072 (1936)
7. F.W.C. Boswell. Proc. Phys. Soc. A64, p.465 (1951)
8. J.S. Halliday, T.B. Rymer and K.H.R. Wright. Proc. Roy. Soc. A225, p.548 (1954)
9. Yu.F. Komnik. Soviet Phys. Solid state. vol.6. No.2. p.479 (1964)
10. R.W. Vook, T. Parker and D. Wright. Sagamore Conference on Physical and Chemical Characteristics of Surfaces and Intersurfaces (Syracouse Univ. press - 1967) p.347
11. R.W. Vook and M.A. Otooni. Ibid.
12. C.W. Mays, J.S. Vermaak and D. Kuhlman - Wilsdorf. Surface, Sci. 12, p.128 (1968)
13. D.C. Smart, F.W. Boswell and J.M. Corbett. J. Appl. Phys. v43, No.11. p.4461 (1972)

14. G.C. Benson and K.S. Yun. "The Solid - Gas Interface," edited by E.A. Flood (Dekker, New York, 1967) vol. 1.

15. K.L. Chopra. Thin Film Phenomena Mc Graw Hill (1969)

16. J.J. Bikerman. Phys. Status Solidi 10, p.3 (1965)

17. A. Cimino, P. Porta and M. Valigi. J. of American Ceramic Soc. vol. 49, No. 3. p.152 (1966)

18. R.W. Vook and F. Witt. J. Appl Phys. 36, p.2169 (1965)

19. R.W. Vook and F. Witt. J. Appl Phys. 36, p.2773 (1968)

20. R.W. Hoffman, R.D. Damels and E.C. Grittende. Proc. Phys. Soc. 67B, p.497 (1967)

21. H. Blackburn and D.S. Campbell. Phil. Mag. 8, p.823 (1963)

22. D.W. Pashley and M.J. Stowell. Phil. Mag. 10, p.127 (1964)

23. A.M. Schwartzman and C.D. Antonio. Thin Solid Films, 2, p.247 (1968)

24. F.C. Frank and J.H. Van Der Merwe. Proc. Roy. Soc. A198:205, p.216 (1949)

25. J.H. Van Der Merwe. Phil. Mag. 7, p.1433 (1962)

26. J.H. Van Der Merwe. J. Appl Phys. 34, p.117 (1963)

27. J.H. Van Der Merwe. J. Appl Phys. 34, p.123 (1963)

28. J.H. Van Der Merwe. J. Appl Phys. 34, p.3420 (1963)

29. J.P. Jones. Proc. Roy. Soc. A284 p.469 (1965)

30. J.W. Matthews. Phil. Mag. 13, p.1207 (1966)

31. J.W. Matthews. and W.A. Jesser. Acta Met. 15, p.595 (1967)

32. W.A. Jesser. and J.W. Matthews. Phil. Mag. 16, p.475 (1968)

33. W.A. Jesser. and J.W. Matthews. Phil. Mag. 16, p.595 (1968)

34. W.A. Jesser. and J.W. Matthews. Phil. Mag. 16, p.461 (1968)

35. J.S. Halliday, T.B. Rymer and K.H.R. Wright. Proc. Roy. Soc. A225, p.548 (1954)

36. J. Riesenfield. and R.W. Hoffman. Case Inst. Tech. AEC Tech. Rept. 32 (1964)

37. D.H. Bradhurst. and J.S.L. Leach. J. Electrochem. Soc. 113, p.1245 (1966)

38. E. Klokholm. and B.S. Berry. J. Electrochem. Soc. 115, p.823 (1968)

39. M.L. Gimpl, A.D. McMaster and N. Fuschillo. J. Appl Phys. 35, p.3572 (1964)

40. C. Gurney. Proc. Phys. Soc. A62, p.639 (1949)

41. D.O. Smith, M.S. Cohen , J. Appl. Phys. 31, p.1775 (1960)

42. G.P. Weiss and D.O. Smith. J. Appl Phys. 33, p.163 (1962)

43. J.D. Finnegan and R.W. Hoffman. AEC Tech. Rept. 18, Case Institute of Technology, Ohio. (1961)

44. T.B. Rymer, F.J. Fayers and S.J. Hewitt.
Proc. Phys. Soc. B69, p.1059 (1956)
45. H.J. Wasserman, J.S. Vermaak. Surface Science 32,
p. 168 (1972)
46. J.H.J. Wasserman and J.S. Vermaak.
Surface Science 22, p.164 (1970)
47. J. Gnan. Ann. Physics. 20, p.361 (1934)
48. G.G. Libowitz and S.H. Bauer. J. Chem. Phys. 58,
p.209 (1954)
49. D.G. Archard. Brit. J. Appl. Phys. 5, p.19 (1954)
50. T.B. Rymer. Nuovo Cimento. No.1, p.294 (1957).
51. N.A. Shishalon Phys. Z. Sowjet. 12, p.20 (1937)
52. T.B. Rymer. Proc. Roy. Soc. A235, p.274 (1956)
53. K. Meyerhoff. Zeit. Fur Naturforshung. IZa, p.23 (1957)
54. H. Levinstein. J. Appl. Phys. 20, p.306 (1949)
55. G. Hass and N. Scott. J. Phys. Rad. 11, p.394 (1950)
56. A.R. Stokes. Proc. Phys. Soc. 61, p.382 (1948)
57. A.J.C. Wilson. Proc. Roy. Soc. A180, p.277 (1942)
58. B.L. Averbach and B.E. Warren. J. Appl. Phys. 20,
p.885 (1949)
59. T.R. Anautharaman and J.W. Christian. Acta Cryst. 9,
p.479 (1956)
60. G.B. Mitra. Acta Cryst. 18, p.393 (1965).
61. G.B. Mitra and N.K. Mistra. Brit. J. Appl. Phys.

17, p.1319 (1966)

62. B.Y. Pines. Dokl. Akad. Nauk SSSR. 103, p.601 (1953)

63. A. Gangulee and C.J.Jr Tomco. Rev. Sci. Instrum. 44, p.909 (1973)

64. A. Gangulee. J. Appl. Cryst. 7, p.439 (1974).

65. T.B. Rymer and C.C. Butler. Phil. Mag. 36, p.515 p.821 (1945)

66. L. Marton and S.H. Lachenbruch. J. Appl. Phys. 20, p.1171 (1949)

67. M.E. Hale, Fuller and Rubinstein. J. Appl. Phys. 30, p.789 (1959)

68. H. Mahl and W. Weitsch. Naturwissenschaften. 46, p.487 (1959)

69. T. Komoda and S. Hosoki. Kyoto Electromagnetic Conf. Report v.1. p.35 (1966)

70. H.U. Fuller and M.E. Hale. J. Appl. Phys. 31, p.238 (1960)

71. G.H. Curtis and R.P. Ferrier. Brit. J. Appl. Phys. v.21. p.1035 (1969)

72. V. Drakos and [illegible] Delong. Czech. J. Phys. B15, p.760 (1965)

73. D.B. Dove. 5. Appl. Phys. 35, p.1652 (1964)

74. C.H. De Tourreil and K.D. Srivastava. IEEE Trans. on Electrical Insulation V. E1-8, p.17 (1973)

75. G.I. Finch and H. Wilman, J. Chem. Soc. 751, p.1937,(1934)

76. V.E. Cosslett, Nature Lond., 136, p.988, (1935)

VITA AUCTORIS

Born in January 1951 in Athens Greece. Completed Primary education in Athens. Moved to Sydney Australia in 1963 and attended the Bondi Junior High school, forms 1 to 4. Returned to Greece in 1966, and in 1968 Graduated from Officers Hill High school Athens. In 1969 moved back to Melbourne Australia and in December 1973 graduated from the Royal Melbourne Institute of Technology with B.Sc in Applied Physics. Came to University of Windsor in May 1974, and completed the present work towards an M.Sc in June 1975.